LETTER

https://doi.org/10.1038/s41586-019-0920-1

The CH25H–CYP7B1–RORα axis of cholesterol metabolism regulates osteoarthritis

Wan-Su Choi[1,7], Gyuseok Lee[1,2,7], Won-Hyun Song[2], Jeong-Tae Koh[2], Jiye Yang[1], Ji-Sun Kwak[1], Hyo-Eun Kim[1], Seul Ki Kim[1], Young-Ok Son[1], Hojung Nam[3], Iljung Jin[3], Zee-Yong Park[4], Jiyeon Kim[4], In Young Park[5], Jeong-Im Hong[5], Hyun Ah Kim[5], Churl-Hong Chun[6], Je-Hwang Ryu[2]* & Jang-Soo Chun[1]*

Osteoarthritis—the most common form of age-related degenerative whole-joint disease[1]—is primarily characterized by cartilage destruction, as well as by synovial inflammation, osteophyte formation and subchondral bone remodelling[2,3]. However, the molecular mechanisms that underlie the pathogenesis of osteoarthritis are largely unknown. Although osteoarthritis is currently considered to be associated with metabolic disorders, direct evidence for this is lacking, and the role of cholesterol metabolism in the pathogenesis of osteoarthritis has not been fully investigated[4–6]. Various types of cholesterol hydroxylases contribute to cholesterol metabolism in extrahepatic tissues by converting cellular cholesterol to circulating oxysterols, which regulate diverse biological processes[7,8]. Here we show that the CH25H–CYP7B1–RORα axis of cholesterol metabolism in chondrocytes is a crucial catabolic regulator of the pathogenesis of osteoarthritis. Osteoarthritic chondrocytes had increased levels of cholesterol because of enhanced uptake, upregulation of cholesterol hydroxylases (CH25H and CYP7B1) and increased production of oxysterol metabolites. Adenoviral overexpression of CH25H or CYP7B1 in mouse joint tissues caused experimental osteoarthritis, whereas knockout or knockdown of these hydroxylases abrogated the pathogenesis of osteoarthritis. Moreover, retinoic acid-related orphan receptor alpha (RORα) was found to mediate the induction of osteoarthritis by alterations in cholesterol metabolism. These results indicate that osteoarthritis is a disease associated with metabolic disorders and suggest that targeting the CH25H–CYP7B1–RORα axis of cholesterol metabolism may provide a therapeutic avenue for treating osteoarthritis.

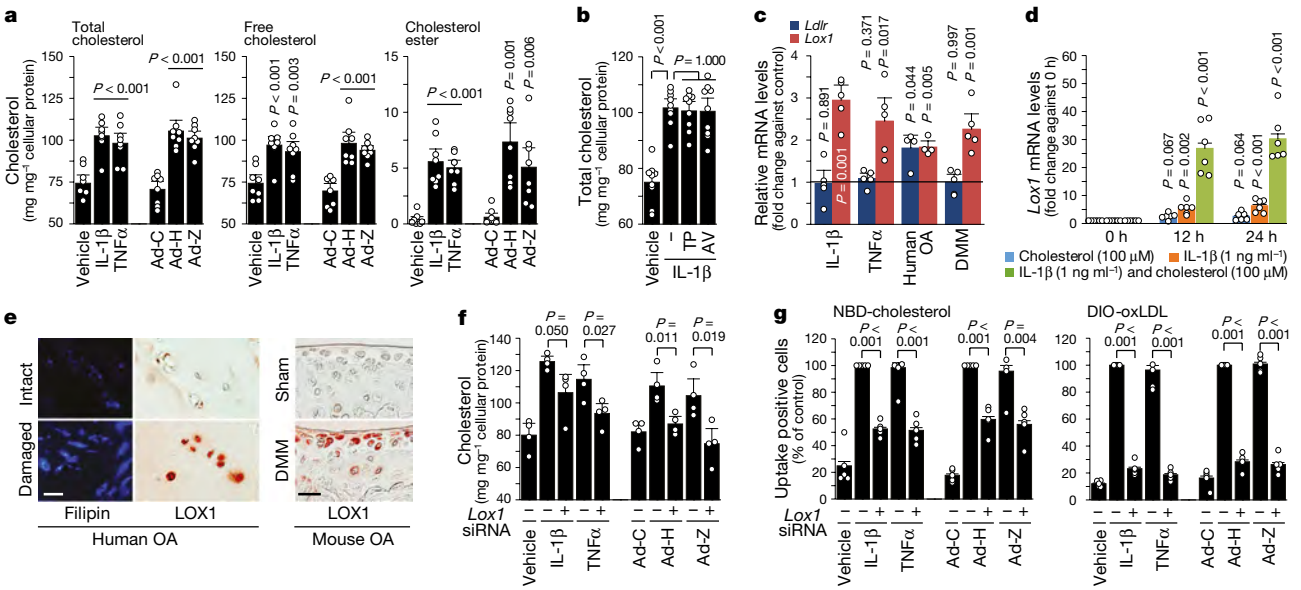

Fig. 1 | OA chondrocytes show increased cholesterol levels via enhanced uptake. a, Levels of total cholesterol, free cholesterol and cholesterol ester in chondrocytes treated with IL-1β (5 ng ml^{-1}) or TNFα (50 ng ml^{-1}) or infected with 800 multiplicity of infection (MOI) of Ad-C (control), Ad-HIF-2α (Ad-H) or Ad-ZIP8 (Ad-Z) for 36 h ($n = 8$). **b**, Total cholesterol levels in chondrocytes treated with IL-1β and the cholesterol synthesis inhibitors triparanol (TP, 5 μM) or atorvastatin (AV, 10 μM), for 36 h ($n = 9$). **c**, *Ldlr* and *Lox1* mRNA levels in chondrocytes treated with IL-1β or TNFα ($n = 5$) or in damaged regions of cartilage from humans with OA (compared with corresponding undamaged regions; $n = 4$) and cartilage from mice with OA induced by DMM (compared with sham operation; $n = 5$). **d**, *Lox1* mRNA levels in chondrocytes treated with cholesterol and/or IL-1β ($n = 6$). **e**, Filipin staining to detect cholesterol in cartilage from humans with OA and LOX1 immunostaining in cartilage from humans ($n = 6$) and mice ($n = 6$) with OA. Scale bars, 25 μm. **f**, **g**, Cholesterol levels (**f**; $n = 4$) and uptake of NBD-cholesterol and DIO-oxLDL (**g**; $n = 5$) in chondrocytes treated as in **a** with or without *Lox1* siRNA. Data are mean ± s.e.m. *n* indicates the number of biologically independent samples, mice per group or human specimens. Two-tailed *t*-test (**a**, **c**, **f**, **g**) and one-way ANOVA with Bonferroni test (**b**, **d**). Exact *P* values (for $P < 0.001$) can be found in the accompanying Source Data.

[1]National Creative Research Initiatives Center for Osteoarthritis Pathogenesis and School of Life Sciences, Gwangju Institute of Science and Technology, Gwangju, South Korea. [2]Department of Pharmacology and Dental Therapeutics, School of Dentistry, Chonnam National University, Gwangju, South Korea. [3]School of Electrical Engineering and Computer Science, Gwangju Institute of Science and Technology, Gwangju, South Korea. [4]School of Life Sciences, Gwangju Institute of Science and Technology, Gwangju, South Korea. [5]Division of Rheumatology, Hallym University Sacred Heart Hospital, Kyunggido, South Korea. [6]Department of Orthopedic Surgery, Wonkwang University School of Medicine, Iksan, South Korea. [7]These authors contributed equally: Wan-Su Choi, Gyuseok Lee. *e-mail: jesryu@jnu.ac.kr; jschun@gist.ac.kr

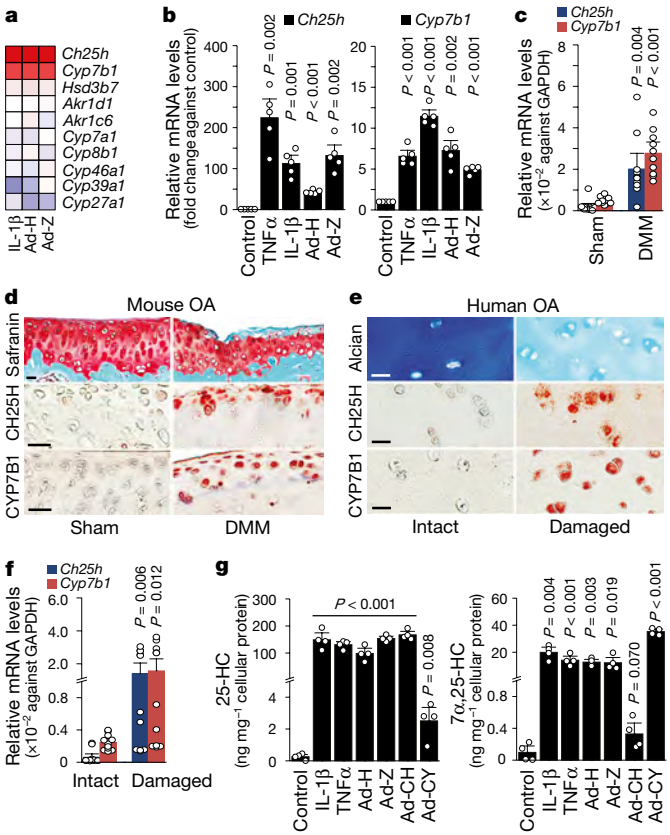

Fig. 2 | Upregulation of the cholesterol hydroxylases CH25H and CYP7B1 and production of their oxysterol metabolites in OA chondrocytes. a, Microarray analysis in chondrocytes treated with IL-1β (1 ng ml^{-1}) or infected with 800 MOI of Ad-HIF-2α (Ad-H) or Ad-ZIP8 (Ad-Z; $n = 4$). Heat map of genes involved in cholesterol metabolism. **b**, *Ch25h* and *Cyp7b1* mRNA levels ($n = 5$) in chondrocytes treated with TNFα (50 ng ml^{-1}) or IL-1β (1 ng ml^{-1}), or infected with 800 MOI of Ad-C (control), Ad-HIF-2α or Ad-ZIP8. **c**, **d**, mRNA levels (**c**) and immunostaining (**d**) for CH25H and CYP7B1 in cartilage tissue from sham- or DMM-operated mice ($n = 11$ mice for sham, 10 mice for DMM). **e**, **f**, Immunostaining (**e**) and mRNA levels (**f**) for CH25H and CYP7B1 in cartilage from humans with OA ($n = 10$). **g**, Oxysterol levels ($n = 4$) in chondrocytes treated with IL-1β (1 ng ml^{-1}) or TNFα (50 ng ml^{-1}) or infected with 800 MOI of Ad-C, Ad-HIF-2α, Ad-ZIP8, Ad-CH25H (Ad-CH) or Ad-CYP7B1 (Ad-CY). Means ± s.e.m. with two-tailed *t*-test. *n* indicates the number of biologically independent samples, mice per group or human specimens. Exact *P* values can be found in the accompanying Source Data. Scale bars, 25 μm.

Although osteoarthritis (OA) has been associated with metabolic syndrome, direct evidence for this link is lacking[5,6]. To address this question, we investigated whether a high-cholesterol diet (HCD)—compared with a regular diet—affects experimental OA in mice, and found that mice fed with an HCD exhibited increased serum cholesterol levels and increased severity of OA caused by destabilization of the medial meniscus (DMM) (Extended Data Fig. 1a). We therefore explored the possible association of OA pathogenesis with cholesterol levels in articular chondrocytes. We measured cholesterol levels in primary cultures of mouse chondrocytes stimulated with interleukin-1β (IL-1β) or tumour necrosis factor-α (TNFα)[9], both of which are OA-associated pro-inflammatory cytokines, and in cells infected with adenoviruses overexpressing HIF-2α (Ad-HIF-2α)[10] or ZIP8 (Ad-ZIP8)[11], which are cellular catabolic regulators of OA. All of these treatments substantially increased the levels of total cholesterol, free cholesterol and cholesterol ester compared with untreated cells (Fig. 1a, Extended Data Fig. 1b, c). Cellular cholesterol homeostasis is regulated by the synthesis, influx, efflux and metabolism of cholesterol[7]. The increase in cholesterol levels in treated cells was not altered by inhibition of cholesterol synthesis, and there were no meaningful changes in the levels of mRNAs encoding proteins involved in cholesterol synthesis or efflux (Fig. 1b, Extended Data Fig. 1d, e). However, the level of mRNA encoding LOX1 (lectin-type oxidized low density lipoprotein receptor 1), which is involved in cholesterol uptake[7,12], was substantially increased in cytokine-stimulated chondrocytes and in the cartilage of humans or mice with OA (Fig. 1c). Treatment with IL-1β and cholesterol synergistically increased *Lox1* mRNA levels in chondrocytes (Fig. 1d). The level of LOX1 protein was also increased in cartilage in humans and mice with OA, coincident with the increase in cellular cholesterol levels (Fig. 1e, Extended Data Fig. 1f). Knockdown of *Lox1* (also known as *Olr1*) using small inhibitory RNA (siRNA) inhibited the increases in cellular cholesterol and the uptake of the fluorescent cholesterol analogue NBD-cholesterol and 3,3′-dioctadecyloxacarbocyanine-oxidized low density lipoprotein (DIO-oxLDL) (Fig. 1f, g, Extended Data Fig. 1g). These results indicate that OA-associated catabolic signalling stimulates LOX1-mediated cholesterol uptake in chondrocytes.

Next, we investigated whether cholesterol metabolism is associated with OA. Using microarray analyses of cholesterol metabolism-related genes in chondrocytes, we found that the genes encoding the cholesterol hydroxylases CH25H (cholesterol 25-hydroxylase) and CYP7B1 (25-hydroxycholesterol 7α-hydroxylase) were prominently upregulated in chondrocytes stimulated with IL-1β, Ad-HIF-2α or Ad-ZIP8 (Fig. 2a, Extended Data Fig. 2a–c). CH25H converts cholesterol to 25-hydroxycholesterol (25-HC) and CYP7B1 metabolizes 25-HC to 7α,25-HC[13]. Quantitative PCR with reverse transcription (qRT–PCR) confirmed the increases in *Ch25h* and *Cyp7b1* mRNA (Fig. 2b, Extended Data Fig. 2d, e). Protein and mRNA levels of CH25H and CYP7B1 were also markedly increased in the cartilage of mice with DMM-induced post-traumatic OA (Fig. 2c, d) and of mice with OA induced by intra-articular injection of Ad-HIF-2α or Ad-ZIP8 (Extended Data Fig. 2f). Because overexpression of HIF-2α or ZIP8 causes spontaneous OA in the absence of mechanical stress, and because mice in which these proteins are transgenically expressed specifically in the cartilage develop OA upon ageing[10,11], we regarded these as models of age-associated OA. Cartilage from humans with OA also exhibited increased CH25H and CYP7B1 mRNA and protein levels (Fig. 2e, f). Moreover, upregulation of CH25H and CYP7B1 resulted in the production of 25-HC and 7α,25-HC, respectively (Fig. 2g, Extended Data Fig. 3). Together, these results indicate that OA chondrocytes show increases in cholesterol uptake, cholesterol hydroxylase levels and oxysterol metabolite production.

We investigated the in vivo activity of CH25H during the pathogenesis of OA using adenovirus (Ad-CH25H)-mediated overexpression and genetic ablation of CH25H in mice. Intra-articular injection of Ad-CH25H resulted in the effective overexpression of CH25H in cartilage, meniscus and synovium and, within three weeks, caused a loss of cartilage glycosaminoglycans and synovitis (Extended Data Fig. 4a, b). Severe cartilage erosion with osteophyte development and thickening of the subchondral bone plate, suggestive of sclerosis, were observed eight weeks after injection (Fig. 3a), which indicates that overexpression of CH25H in joint tissues is sufficient to cause OA. We further validated the catabolic role of CH25H using *Ch25h*$^{-/-}$ mice, which exhibit normal skeletal development[14] and an absence of CH25H protein (Extended Data Fig. 4c–e). The DMM-induced upregulation of CH25H and the production of the aggrecan neoepitopes DIPEN and NITEGE[15] in the cartilage were reduced in *Ch25h*$^{-/-}$ mice when compared with wild-type mice (Extended Data Fig. 4f). Similarly, manifestations of DMM-induced OA (cartilage destruction, osteophyte formation and thickening of the subchondral bone plate) were substantially inhibited in *Ch25h*$^{-/-}$ mice, compared with wild-type mice, 8 and 12 weeks after DMM (Fig. 3b, c, Extended Data Fig. 4g). We also examined the functions of CH25H in mice fed with an HCD and subjected to DMM surgery, as a model of metabolism-associated post-traumatic OA. Compared with mice fed a regular diet, mice fed with an HCD exhibited more severe OA manifestations four and six weeks after surgery,

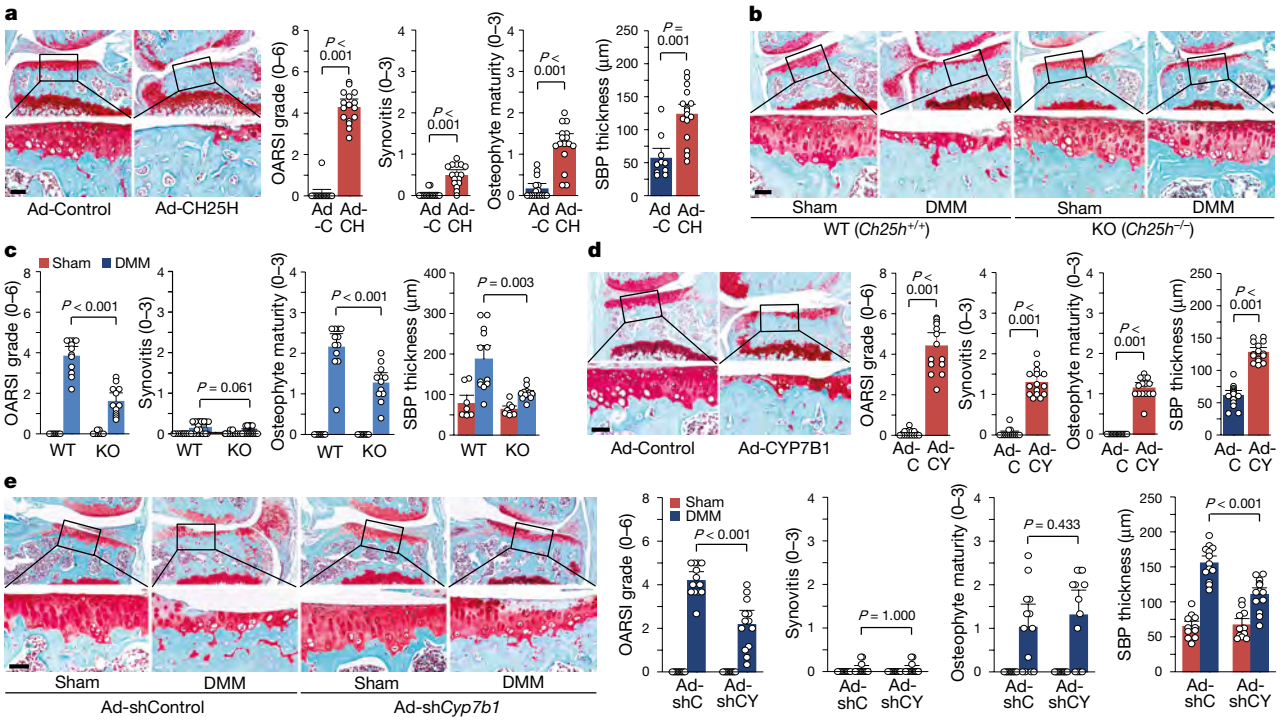

Fig. 3 | CH25H and CYP7B1 regulate pathogenesis of OA in mice. Experimental OA was examined by safranin-O staining and scoring of OA parameters, including cartilage destruction (OARSI grade), synovitis, osteophyte maturity and thickening of the subchondral bone plate (suggestive of sclerosis). **a**, Safranin-O staining and scoring of OA parameters in wild-type mice that had undergone intra-articular injection of Ad-C ($n = 10$ mice) or Ad-CH25H (Ad-CH; $n = 15$ mice) for 8 weeks. **b**, **c**, Safranin-O staining (**b**) and scoring of OA parameters (**c**) in sham- or DMM-operated *Ch25h*$^{-/-}$ and wild-type littermates ($n = 8$ mice for sham and 12 mice for DMM). **d**, Safranin-O staining and scoring of OA parameters from wild-type mice that had undergone intra-articular injection of Ad-C ($n = 15$ mice) or Ad-CYP7B1 (Ad-CY; $n = 15$ mice). **e**, Safranin-O staining and scoring of OA parameters in mice subjected to sham operation ($n = 10$ mice) or DMM surgery ($n = 15$ mice) and intra-articular injection of Ad-shControl (Ad-shC) or Ad-sh*Cyp7b1* (Ad-shCY). Means ± 95% confidence interval (CI) with Mann–Whitney *U* test for OARSI grade, synovitis and osteophyte maturity; means ± s.e.m. with two-tailed *t*-test for SBP thickness. Exact *P* values can be found in the accompanying Source Data. Scale bars, 25 μm.

and these manifestations were inhibited in *Ch25h*$^{-/-}$ mice (Extended Data Fig. 4h). The DMM-induced OA pain seen in wild-type mice was also significantly reduced in *Ch25h*$^{-/-}$ mice (Extended Data Fig. 4i).

We also investigated the in vivo functions of CYP7B1 by overexpressing it or knocking it down in mouse joint tissues. Intra-articular injection of Ad-CYP7B1 resulted in the overexpression of CYP7B1 in joint tissues (Extended Data Fig. 5a), synovitis and loss of cartilage glycosaminoglycans three weeks after injection (Extended Data Fig. 5b), and osteophyte development, subchondral bone sclerosis and severe cartilage destruction eight weeks after injection (Fig. 3d). We further validated the role of CYP7B1 by knocking it down in whole-joint tissues via intra-articular injection of an adenovirus-encoded short hairpin (sh)RNA, Ad-sh*Cyp7b1*, which markedly decreased CYP7B1 protein in cartilage tissue (Extended Data Fig. 5c). Knockdown of CYP7B1 also triggered substantial reductions in DMM-induced or metabolism-associated post-traumatic OA and OA pain (Fig. 3e, Extended Data Fig. 5d–g). Although DMM-induced osteophyte maturity was not affected by Ad-sh*Cyp7b1*, these results collectively indicate that both CH25H and CYP7B1 are necessary for experimental OA in mice.

Because OA chondrocytes exhibit upregulation of matrix-degrading enzymes and/or downregulation of extracellular matrix molecules[16], we tested whether cholesterol metabolism regulates the expression of relevant effector molecules. We found that cholesterol and its metabolites upregulated the matrix metallopeptidases MMP3, MMP12 and MMP13, whereas SOX9, type II collagen and aggrecan were downregulated by 25-HC but not by cholesterol or 7α,25-HC. Similarly, overexpression of CH25H or CYP7B1 upregulated MMP3, MMP12 and MMP13, whereas overexpression of CYP7B1 upregulated the aggrecanase ADAMTS5 and downregulated anabolic factors (Extended Data Fig. 6a). Genetic knockout studies in mice showed that MMP3, MMP13 and ADAMTS5 are crucial effector molecules for cartilage destruction in OA[17–19], which suggests that the upregulation of MMP3 and MMP13 contributes to cartilage destruction in OA caused by cholesterol metabolism. Indeed, the secreted protein levels of MMP3 and MMP13 were increased by cholesterol metabolism (Extended Data Fig. 6b) and the levels of these proteins were markedly reduced in the cartilage of *Ch25h*$^{-/-}$ mice and mice that had undergone intra-articular injections of Ad-sh*Cyp7b1*, when compared with DMM-operated wild-type mice (Extended Data Fig. 6c). In addition, adenoviral overexpression of CH25H or CYP7B1 induced the production of DIPEN and NITEGE in cartilage tissue, as did DMM surgery, with the latter effect being enhanced in the cartilage of mice fed with an HCD (Extended Data Fig. 6d, e). These results suggest that cholesterol metabolism exerts a catabolic function in chondrocytes by upregulating matrix-degrading enzymes.

To identify downstream mediators of cholesterol metabolism, we examined the expression of putative receptors for cholesterol and oxysterols, including ROR, LXR (liver X receptor) and ESR1 (oestrogen receptor 1)[20–22]. Among them, only RORα was upregulated in all chondrocytes stimulated with cytokines, cholesterol and oxysterols, and in cartilage from humans or mice with OA (Extended Data Fig. 7a). IL-1β and TNFα increased RORα and decreased RORγ expression in cultured primary chondrocytes, whereas RORβ was barely detectable (Extended Data Fig. 7b). Similarly, cartilage from humans or mice with OA exhibited increased RORα and decreased RORγ (Extended Data Fig. 7c, d). Furthermore, the transcriptional activity of RORα was substantially increased by OA-associated catabolic signalling (Fig. 4a) and by cholesterol, 25-HC and 7α,25-HC, all of which act as direct binding ligands of RORα (Extended Data Fig. 7e). These results suggest that RORα is a downstream target of the CH25H–CYP7B1 axis

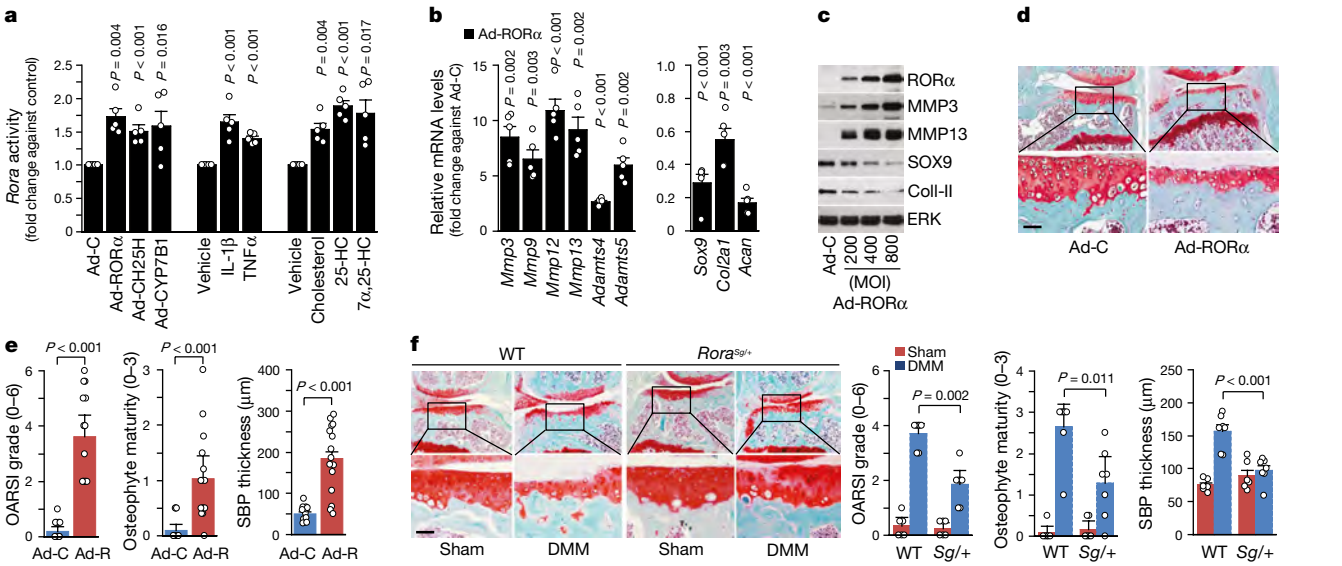

Fig. 4 | RORα mediates pathogenesis of cholesterol metabolism-induced OA. a, *Rora* reporter gene activity in chondrocytes infected with 800 MOI of Ad-C, Ad-RORα, Ad-CH25H or Ad-CYP7B1, or treated with IL-1β (1 ng ml^{-1}), TNFα (50 ng ml^{-1}), MβCD-cholesterol (100 μM), 25-HC (20 μM) or 7α,25-HC (800 nM) ($n = 5$). **b**, **c**, qRT–PCR analysis of mRNA levels (**b**) and western blotting of protein levels (**c**) of the indicated molecules in chondrocytes infected with Ad-C (800 MOI) or Ad-RORα ($n = 5$). **d**, **e**, Safranin-O staining (**d**) and scoring of OA parameters (**e**) in mice that had undergone intra-articular injection with Ad-C or Ad-RORα once weekly for three weeks and mice were euthanized eight weeks after the first injection ($n = 15$). **f**, Safranin-O staining and scoring of OA parameters in *Rora*$^{Sg/+}$ and wild-type littermates subjected to sham ($n = 6$) and DMM ($n = 7$) operations. Means ± s.e.m. with two-tailed *t*-test (**a**, **b**). Means ± 95% CI with Mann–Whitney *U* test for OARSI grade and osteophyte maturity and means ± s.e.m. with two-tailed *t*-test for SBP thickness (**e**, **f**). *n* indicates the number of biologically independent samples or mice per group. Exact *P* values can be found in the accompanying Source Data. For gel source data, see Supplementary Fig. 1. Scale bars, 25 μm.

of cholesterol metabolism. Furthermore, adenoviral overexpression of RORα upregulated MMP3, MMP9, MMP12, MMP13, ADAMTS4 and ADAMTS5, and downregulated the expression of the anabolic factors SOX9, collagen-II and aggrecan (Fig. 4b, c, Extended Data Fig. 7f). Chromatin immunoprecipitation assays revealed that RORα directly regulates the expression of MMP3, MMP13 and ADAMTS5 (Extended Data Fig. 7g).

The functions of RORα in OA were examined by intra-articular injection of Ad-RORα, which induced RORα expression in joint tissues and the production of DIPEN and NITEGE neoepitopes in cartilage, and triggered all examined OA phenotypes (Fig. 4d, e, Extended Data Fig. 8a). The chondrocyte-specific function of RORα was examined by generating RORα transgenic mice using the *Col2a1* promoter and enhancer[10,11]; these transgenic mice exhibited enhanced DMM-induced OA compared with wild-type mice (Extended Data Fig. 8b, c). We confirmed the functions of RORα using staggerer mice (*Rora*$^{Sg/Sg}$), which lack the RORα ligand-binding domain[23]. As homozygous *Rora*$^{Sg/Sg}$ mice exhibit phenotypes similar to RORα-knockout mice, including postnatal lethality[24], we used *Rora*$^{Sg/+}$ mice for experimental OA. *Rora*$^{Sg/+}$ mice exhibited normal skeletal development with markedly reduced RORα levels (Extended Data Fig. 9a–d). DMM-induced OA manifestations were substantially reduced in *Rora*$^{Sg/+}$ mice 8 and 12 weeks after DMM (Fig. 4f, Extended Data Fig. 9e). In addition, all OA manifestations were enhanced in mice fed with an HCD, and this effect was substantially reduced in *Rora*$^{Sg/+}$ mice (Extended Data Fig. 9f). We further validated the role of RORα using SR3335, an inverse agonist of RORα[25]. Intra-articular injection of SR3335 substantially reduced the cartilage destruction caused by Ad-RORα or DMM surgery, and inhibited the upregulation of MMP3 and MMP13 caused by cholesterol and its metabolites (Extended Data Fig. 9g–i). Collectively, these results suggest that RORα mediates the pathogenesis of OA caused by alteration of cholesterol metabolism in mice.

We also evaluated the CH25H–CYP7B1–RORα axis of cholesterol metabolism in other cell types found in joint tissues, specifically fibroblast-like synoviocytes and the macrophage cell line Raw264.7. Although these cells showed increased cholesterol levels due to OA-associated catabolic signalling, they did not exhibit the cholesterol metabolism pathway in question (Extended Data Fig. 10a–g). We also verified the relevance of our findings to humans by examining the CH25H–CYP7B1–RORα axis of cholesterol metabolism in normal human chondrocytes, and found that this pathway functions in normal human chondrocytes (Extended Data Fig. 10h). Unlike cartilage, synovial tissue from humans with OA showed low levels of expression of CH25H, CYP7B1 and RORα (Extended Data Fig. 10i), further supporting the idea that the CH25H–CYP7B1–RORα axis of cholesterol metabolism has a cartilage-specific function.

Various epidemiologic studies have suggested a correlation between human serum cholesterol levels and OA[26–28]. To date, however, the role of cholesterol metabolism in OA pathogenesis has not been clearly determined. A recent report[29] indicated that stimulation of cholesterol synthesis in chondrocytes by double knockout of *Insig1* and *Insig2* increased the severity of OA in mice, which suggests that modulation of intracellular cholesterol levels is an important regulatory factor in the pathogenesis of OA. We have shown that increased levels of cholesterol in chondrocytes via LOX1-mediated enhanced uptake and its metabolism by CH25H and CYP7B1 cause experimental OA in mice. We have also shown that the interaction between cholesterol metabolism and RORα is important in the pathogenesis of OA. Specifically, cholesterol and its oxysterol metabolites directly activate RORα, which causes OA pathogenesis—at least in part by upregulating matrix-degrading enzymes in chondrocytes.

Online content

Any methods, additional references, Nature Research reporting summaries, source data, statements of data availability and associated accession codes are available at https://doi.org/10.1038/s41586-019-0920-1.

Received: 23 October 2017; Accepted: 8 January 2019;
Published online 6 February 2019.

1. Hunter, D. J., Schofield, D. & Callander, E. The individual and socioeconomic impact of osteoarthritis. *Nat. Rev. Rheumatol.* **10**, 437–441 (2014).
2. Loeser, R. F., Goldring, S. R., Scanzello, C. R. & Goldring, M. B. Osteoarthritis: a disease of the joint as an organ. *Arthritis Rheum.* **64**, 1697–1707 (2012).

3. Moon, P. M. & Beier, F. Novel insights into osteoarthritis joint pathology from studies in mice. *Curr. Rheumatol. Rep*. **17**, 50 (2015).
4. Mobasheri, A. et al. The role of metabolism in the pathogenesis of osteoarthritis. *Nat. Rev. Rheumatol*. **13**, 302–311 (2017).
5. Niu, J., Clancy, M., Aliabadi, P., Vasan, R. & Felson, D. T. Metabolic syndrome, its components, and knee osteoarthritis: the Framingham osteoarthritis study. *Arthritis Rheumatol*. **69**, 1194–1203 (2017).
6. Courties, A., Sellam, J. & Berenbaum, F. Metabolic syndrome-associated osteoarthritis. *Curr. Opin. Rheumatol*. **29**, 214–222 (2017).
7. Goedeke, L. & Fernández-Hernando, C. Regulation of cholesterol homeostasis. *Cell. Mol. Life Sci*. **69**, 915–930 (2012).
8. Olkkonen, V. M., Béaslas, O. & Nissilä, E. Oxysterols and their cellular effectors. *Biomolecules* **2**, 76–103 (2012).
9. Kapoor, M., Martel-Pelletier, J., Lajeunesse, D., Pelletier, J. P. & Fahmi, H. Role of proinflammatory cytokines in the pathophysiology of osteoarthritis. *Nat. Rev. Rheumatol*. **7**, 33–42 (2011).
10. Yang, S. et al. Hypoxia-inducible factor-2α is a catabolic regulator of osteoarthritic cartilage destruction. *Nat. Med*. **16**, 687–693 (2010).
11. Kim, J. H. et al. Regulation of the catabolic cascade in osteoarthritis by the zinc–ZIP8–MTF1 axis. *Cell* **156**, 730–743 (2014).
12. Zeya, B., Arjuman, A. & Chandra, N. C. Lectin-like oxidized low-density lipoprotein (LDL) receptor (LOX-1): a chameleon receptor for oxidized LDL. *Biochemistry* **55**, 4437–4444 (2016).
13. Cyster, J. G., Dang, E. V., Reboldi, A. & Yi, T. 25-Hydroxycholesterols in innate and adaptive immunity. *Nat. Rev. Immunol*. **14**, 731–743 (2014).
14. Reboldi, A. et al. Inflammation. 25-Hydroxycholesterol suppresses interleukin-1-driven inflammation downstream of type I interferon. *Science* **345**, 679–684 (2014).
15. Roughley, P. J. & Mort, J. S. The role of aggrecan in normal and osteoarthritic cartilage. *J. Exp. Orthop*. **1**, 8 (2014).
16. Troeberg, L. & Nagase, H. Proteases involved in cartilage matrix degradation in osteoarthritis. *Biochim. Biophys. Acta* **1824**, 133–145 (2012).
17. Blom, A. B. et al. Crucial role of macrophages in matrix metalloproteinase-mediated cartilage destruction during experimental osteoarthritis: involvement of matrix metalloproteinase 3. *Arthritis Rheum*. **56**, 147–157 (2007).
18. Glasson, S. S. et al. Deletion of active ADAMTS5 prevents cartilage degradation in a murine model of osteoarthritis. *Nature* **434**, 644–648 (2005).
19. Little, C. B. et al. Matrix metalloproteinase 13-deficient mice are resistant to osteoarthritic cartilage erosion but not chondrocyte hypertrophy or osteophyte development. *Arthritis Rheum*. **60**, 3723–3733 (2009).
20. Kallen, J. A. et al. X-ray structure of the hRORα LBD at 1.63 Å: structural and functional data that cholesterol or a cholesterol derivative is the natural ligand of RORα. *Structure* **10**, 1697–1707 (2002).
21. Tuong, Z. K. et al. RORα and 25-hydroxycholesterol crosstalk regulates lipid droplet homeostasis in macrophages. *PLoS ONE* **11**, e0147179 (2016).
22. Guillemot-Legris, O., Mutemberezi, V. & Muccioli, G. G. Oxysterols in metabolic syndrome: from bystander molecules to bioactive lipids. *Trends Mol. Med*. **22**, 594–614 (2016).
23. Hamilton, B. A. et al. Disruption of the nuclear hormone receptor RORα in staggerer mice. *Nature* **379**, 736–739 (1996).
24. Dussault, I., Fawcett, D., Matthyssen, A., Bader, J. A. & Giguère, V. Orphan nuclear receptor RORα-deficient mice display the cerebellar defects of staggerer. *Mech. Dev*. **70**, 147–153 (1998).
25. Kumar, N. et al. Identification of SR3335 (ML-176): a synthetic RORα selective inverse agonist. *ACS Chem. Biol*. **6**, 218–222 (2011).
26. de Munter, W., van der Kraan, P. M., van den Berg, W. B. & van Lent, P. L. High systemic levels of low-density lipoprotein cholesterol: fuel to the flames in inflammatory osteoarthritis? *Rheumatology* **55**, 16–24 (2016).
27. Farnaghi, S., Crawford, R., Xiao, Y. & Prasadam, I. Cholesterol metabolism in pathogenesis of osteoarthritis disease. *Int. J. Rheum. Dis*. **20**, 131–140 (2017).
28. Garcia-Gil, M. et al. Serum lipid levels and risk of hand osteoarthritis: the Chingford Prospective Cohort Study. *Sci. Rep*. **7**, 3147 (2017).
29. Ali, S. A. et al. Regulation of cholesterol homeostasis by Hedgehog signaling in osteoarthritic cartilage. *Arthritis Rheumatol*. **68**, 127–137 (2016).

Acknowledgements This work was supported by grants from the National Research Foundation of Korea (2016R1A3B1906090 and 2016R1A5A1007318 to J.-S.C., 2012R1A5A2A39671455 and 2018R1A2B2006033 to J.-H.R., and 2017R1A6A3A11034719 to W.-S.C.), the Korea Healthcare Technology R&D project of the Korea Health Industry Development Institute (HI16C0287 to J-.S.C., J.-H.R. and H.A.K., and H114C3484 to J.-S.C. and J.-H.R.), and the GIST Research Institute (GRI) to J.-S.C.

Reviewer information *Nature* thanks Benjamin Alman and the other anonymous reviewer(s) for their contribution to the peer review of this work.

Author contributions W.-S.C. and G.L. designed, performed and analysed the experiments. W.-H.S., J.Y., J.-S.K., H.-E.K., S.K.K. and Y.-O.S. assisted with the experimental analyses. H.N. and I.J. performed the bioinformatic analysis. Z.-Y.P. and J.K. carried out the liquid chromatography–tandem mass spectrometry analysis. I.Y.P. and J.-I.H. performed the pain assay. H.A.K., J.-T.K. and C.-H.C. evaluated the human samples and critically revised the manuscript. W.-S.C, G.L., J.-H.R. and J.-S.C wrote the manuscript. J.-H.R. and J.-S.C. conceived, planned and oversaw the study.

Competing interests The authors declare no competing interests.

Additional information
Extended data is available for this paper at https://doi.org/10.1038/s41586-019-0920-1.
Supplementary information is available for this paper at https://doi.org/10.1038/s41586-019-0920-1.
Reprints and permissions information is available at http://www.nature.com/reprints.
Correspondence and requests for materials should be addressed to J.-H.R. or J.-S.C.
Publisher's note: Springer Nature remains neutral with regard to jurisdictional claims in published maps and institutional affiliations.

METHODS

Human subjects. International Cartilage Repair Society (ICRS) grade 4 human OA cartilage tissue was obtained from individuals undergoing arthroplasty (Extended Data Fig. 1f). The Institutional Review Board of Wonkwang University Hospital approved the use of these tissues, and written informed consent was obtained from all patients before the operative procedure. Synovium tissue from humans with OA or rheumatoid arthritis were as previously described[30]. We complied with all relevant ethical regulations and used approved study protocols. Normal primary human chondrocytes were purchased from Cell Applications. Cells were cultured according to the supplier's recommendations. Human chondrocytes were provided at passage 1, and all experiments were conducted on cells at passages 2 and 3.

Mice. C57BL/6 male mice (wild type, *Ch25h*$^{-/-}$ and *Rora*$^{Sg/+}$) were subjected to induction of experimental OA. *Ch25h*$^{-/-}$ mice[14] and *Rora*$^{Sg/+}$ mice (a spontaneous RORα mutant strain[23]) were obtained from the Jackson Laboratory. Homozygous *Rora*$^{Sg/Sg}$ mice exhibit tremors, body imbalance, hypotonia and small size at birth, and die shortly after weaning; by contrast, heterozygous *Rora*$^{Sg/+}$ mice exhibit normal development[24]. We therefore used *Rora*$^{Sg/+}$ mice for our experimental OA studies. Cartilage-specific *Rora* transgenic mice were generated using the *Col2a1* promoter and enhancer, as previously described[10,11]. We used whole-body deletion of *Ch25h* and mutation of *Rora*, as well as intra-articular injection of adenovirus into whole-joint tissues, because OA is a whole-joint disease that involves multiple pathological changes in all joint tissues. All mice were maintained in pathogen-free barrier facilities. For each experiment, sex- and age-matched mice were used and randomly allocated to each experimental group. All experiments using mice were approved by the Gwangju Institute of Science and Technology Animal Care and Use Committee and the Animal Care and Ethics Committees of Chonnam National University. We complied with all relevant ethical regulations and used approved study protocols.

Experimental OA in mice. Experimental OA was induced by DMM surgery in 12-week-old male mice; sham-operated mice were used as controls[31]. Knee joints were processed for histological analysis 8 and 12 weeks after surgery or, for studies involving HCD, 4 and 6 weeks after surgery. Experimental OA was also induced by intra-articular injections into the knee (once weekly for 3 weeks) of adenoviruses, including Ad-HIF-2α, Ad-ZIP8, Ad-CH25H, Ad-CYP7B1 and Ad-RORα (1×10^9 plaque forming units (PFU) in a total volume of 10 μl), into 12-week-old male mice; intra-articular injection of empty adenovirus (Ad-C) was used as a control[10,11,32]. Mice were killed for analysis three or eight weeks after the first injection. Where indicated, Ad-RORα-injected or DMM-operated mice were co-injected (intra-articular) with 7.5 mg kg^{-1} body weight of SR3335 (Cayman Chemicals), an inverse agonist of RORα[25]. To knockdown CYP7B1 in whole-joint tissues, sham- or DMM-operated mice underwent intra-articular injections of Ad-shControl or Ad-sh*Cyp7b1* (1×10^9 PFU in a total volume of 10 μl) 10 days post-operation. All adenoviruses were purchased from Vector Biolabs.

HCD in mice. Male mice (five weeks old) were fed with AIN-76A diet (Feed Laboratory) as the regular diet. For the HCD, mice were fed with a modified AIN-76A diet supplemented with 2% cholesterol. DMM surgery was performed after seven weeks of regular diet or HCD on the right knees of mice. The mice were killed four or six weeks after DMM surgery for histological analysis.

Histology and immunohistochemistry. Cartilage from humans with OA was frozen, sectioned at 10-μm thickness and fixed in 4% paraformaldehyde (PFA). The cartilage sections were stained with Alcian blue, de-stained with 0.1 N HCl, washed twice with distilled water, dried and mounted. For immunohistochemical staining for RORα, LOX1, CH25H and CYP7B1, frozen sections of human cartilage were washed, fixed in 4% (v/v) fresh PFA and stained using an LSAB2 horseradish peroxidase kit (Dako). Slide-mounted sections were then incubated for 2 h at room temperature with antibodies against RORα (Sigma-Aldrich), LOX1 (Abcam), CH25H (Antibodies Online) or CYP7B1 (Thermo Fisher Scientific). The sections were incubated with biotinylated linking and streptavidin-horseradish peroxidase reagents for 10 min. Immunoreactive proteins were visualized using a 3-amino-9-ethylcarbazole (AEC) substrate chromogen solution (Dako). Images were acquired under a Zeiss Axio Scope A1 microscope.

Cartilage destruction in mice was examined using safranin-O staining. In brief, knee joints were fixed in 4% PFA, decalcified in 0.5 M EDTA and embedded in paraffin. The paraffin blocks were sectioned at a thickness of 5 μm. Serial sections were obtained from the entire joint at 80-μm intervals, and the sections were deparaffinized in xylene, hydrated with graded ethanol and stained with safranin-O. Cartilage destruction was scored by blinded observers using the OARSI grading system[10,11,33]. Synovitis was determined by safranin-O and haematoxylin staining, and synovial inflammation (grade 0–3) was scored as previously described[34]. Osteophyte development was identified by safranin-O staining, and osteophyte maturity was quantified as previously described[19]. The thickness of the subchondral bone plate (suggestive of subchondral bone sclerosis) was measured[35]. For immunostaining of mouse joint sections, deparaffinized and hydrated sections were stained using an LSAB2 horseradish peroxidase kit. In brief, sections were incubated overnight at 4 °C with antibodies against RORα (Sigma-Aldrich), LOX1 (Abcam), MMP3 (Abcam), MMP13 (Abcam), CH25H (Antibodies Online), CYP7B1 (Thermo Fisher Scientific), DIPEN (Mybiosource), NITEGE (Novus), HIF-2α (Abcam) or ZIP8 (Santa Cruz). The samples were then incubated with Envision+System HRP-labelled polymer reagents (Dako) for 10 min. Immunoreactive proteins were visualized using AEC High Sensitivity Substrate Chromogen Solution (Dako). Images were acquired under a Zeiss Axio Scope A1 microscope and analysed using Image J software (National Institutes of Health, v.1.51a).

Pain assay. OA-associated pain in the various mouse models was measured using the von Frey assay and the hot-plate assay[36]. These behavioural tests were performed three times before DMM surgery and once every two weeks after surgery. To measure the response latencies in the hot-plate assay, we used a glass cylinder (40-cm high, 20-cm diameter) to keep mice on the hot surface of the plate, which was maintained at a temperature of 55 ± 0.5 °C. The time (s) between placement of the mouse and the onset of paw shaking or licking, or jumping behaviour, was recorded as the index of response latency. A latency period (cut-off) of 30 s was defined as complete analgesia. The test was repeated three times in mice, and the mean values were calculated. Development of mechanical allodynia was assessed every two weeks using von Frey filaments. Mice were placed in a perspex chamber with a metal grid floor that gave access to the underside of their paws, and allowed to acclimate for at least 15 min. Once the mouse had fully acclimatized to the apparatus and ceased exploratory behaviour, mechanical allodynia was tested by touching the plantar surface of the hind paw with von Frey filaments in ascending order of force for up to 6 s. A positive response was noted if the paw was sharply withdrawn or there was flinching upon removal of the hair. The test was repeated three times, and the mean value was calculated.

Cell culture. Primary chondrocytes were isolated from the femoral condyles and tibial plateaus of wild-type and *Ch25h*$^{-/-}$ mice on postnatal day 5, as previously described[37]. Chondrocytes were maintained as a monolayer in Dulbecco's modified Eagle's medium (DMEM) supplemented with 10% fetal bovine serum (FBS) and the appropriate antibiotics. At culture day 3, cells were treated as indicated for each experiment. Mouse fibroblast-like synoviocytes (FLSs) were isolated and cultured as previously described[30]. FLSs of passages 4–8 were used for further analysis. Pure FLSs (>90% CD90$^+$/<1% CD14$^+$) were identified by flow cytometry using antibodies against CD90 and CD14 (Abcam). Mycoplasma-free Raw264.7 cells were obtained from ATCC (TIB-71).

Cholesterol assay. Cellular total cholesterol levels were measured using a Total Cholesterol Assay Kit (Cell Biolabs). In brief, cellular lipids were extracted using chloroform:2-propanol:NP-40 (7:11:0.1) in a micro-homogenizer, and the levels of total cholesterol and free cholesterol were determined according to the manufacturer's instructions. The amount of cholesterol ester was calculated by subtracting the amount of free cholesterol from the amount of total cholesterol. For cholesterol staining of cartilage tissue, frozen sections of human cartilage were washed and fixed in 4% PFA. Slide-mounted sections were incubated overnight at 4 °C with filipin (250 μg ml^{-1}, Sigma-Aldrich). To track the influx of cholesterol-containing lipoproteins into chondrocytes, the cells were treated with DIO-oxLDL (25 μg ml^{-1}, Kalen Biomedical), fixed in 4% fresh PFA, permeabilized with 0.2% Triton X-100 in PBS, blocked with PBS containing 0.1% BSA, washed and incubated with DAPI for 10 min. Cartilage tissue and chondrocytes were observed under a Zeiss Axio Scope A1 microscope connected to a fluorescence unit. Cholesterol uptake was assessed using a Cholesterol Uptake Cell-Based Assay Kit (Cayman Chemicals) and NBD-cholesterol, a fluorescent cholesterol analogue. In brief, chondrocytes were incubated for 36 h in serum-free DMEM containing 20 μg ml^{-1} NBD-cholesterol with or without IL-1β (1 ng ml^{-1}), TNFα (50 ng ml^{-1}), Ad-HIF-2α (800 MOI) or Ad-ZIP8 (800 MOI). At the end of this treatment, the plates were aspirated, the cell-based assay buffer was added to each well, and the uptake of NBD cholesterol was detected using a fluorescent microscope (480-nm excitation and 520-nm emission). Cellular uptake of oxLDL was measured using confocal microscopy. In brief, chondrocytes were incubated for 36 h in serum-free DMEM containing 20 μg ml^{-1} DIO-oxLDL with or without IL-1β, TNFα, Ad-HIF-2α or Ad-ZIP8. At the end of the incubation period, the cells were washed, mounted on coverslips and examined by confocal microscopy. Data were analysed using Image-J software. Cells that were positive for uptake of NBD cholesterol or DIO-oxLDL were quantified and expressed as a percentage of the control.

Liquid chromatography–tandem mass spectrometry analysis of cholesterol metabolites. Primary cultured chondrocytes were treated with vehicle, IL-1β (1 ng ml^{-1}) or TNFα (50 ng ml^{-1}), or were infected with 800 MOI of Ad-C, Ad-HIF-2α or Ad-ZIP8. The levels of intracellular oxysterols were measured by liquid chromatography–tandem mass spectrometry (LC–MS/MS) analysis as described[38]. In brief, primary cultured chondrocytes treated as noted above (3×10^6 in 100 μl of H_2O containing 200 μM butylated hydroxytoluene (BHT)) were lysed with a micro-homogenizer, gradually mixed with 900 μl of EtOH by shaking and then gradually cooled to 4 °C to allow slow precipitation. The extracts were dried under an N_2 steam at 40 °C and resuspended in 10 μl EtOH:H_2O (50:50).

A mixture of reconstituted sample and 100 pmol of deuterated internal standard oxysterols (deuterated 25-HC and deuterated 7α,25-HC; Avanti Polar Lipids) was injected onto an analytical column (fused-silica capillary 100 μm i.d. × 360 μm o.d.; packed with 7.5 cm of Aqua C18), and LC–MS/MS analyses of endogenous oxysterols were carried out using an Agilent 1100 series high-performance liquid chromatography (HPLC) pump (Agilent Technologies) coupled to a linear ion trap mass spectrometer (Thermo Fisher Scientific). For the separation of oxysterols, mobile phase A (5% aqueous MeOH/ 0.1% formic acid; FA) and mobile phase B (MeOH/0.1% FA) were delivered at a flow rate of 250 nl/min. A 15-min linear gradient program from 60–97% phase B followed by a 10-min isocratic elution of 97% B was used. The mass spectrometer was operated in a data-dependent mode with an m/z range of 100–1,000 and a positive polarity. As oxysterols may easily dissociate into several water-labile ion forms during electrospray ionization, the main ions used for quantification were the $[M+H^+-2H_2O]^+$ ion of 7α,25-HC at m/z 383.33, the $[M+H^+-2H_2O]^+$ ion of 7α,25-HC-d6 at m/z 389.37, the $[M+H^+-H_2O]^+$ ion of 25-HC at m/z 385.35 and the $[M+H^+-H_2O]^+$ ion of 25-HC-d6 at m/z 391.38. The peak area of each oxysterol was calculated with the built-in peak area integration feature of Xcalibur v.2.2 (Thermo Fisher Scientific). The peak area of each endogenous oxysterol was normalized to that of its corresponding internal standard to obtain a peak area ratio. The absolute quantitative levels of the native oxysterols were calculated using the obtained peak area ratio multiplied by the injected amount of the internal oxysterol standard.

Microarray analyses. Total RNA was extracted from mouse articular chondrocytes using a Purelink RNA mini kit (Ambion). The concentration, purity and integrity of the extracted RNA were determined by spectrophotometry. Four replicates for each cell type were isolated and processed. RNA from mouse chondrocytes was analysed using Affymetrix Gene Chip arrays (Affymetrix GeneChip Mouse Gene 2.0 ST Array) in accordance with the Affymetrix protocol (Macrogen). Probe signals in the raw data were normalized by the RMA (robust multi-array average) for each separate dataset (IL-1β treatment or injection of Ad-C, Ad-HIF-2α or Ad-ZIP8). Normalization was performed using R v.3.3.2 with Affy package v.1.52.0. To identify differentially expressed genes, we performed Student's t-test followed by the Benjamini–Hochberg multiple hypothesis test for each group using Python v.3.4.3 and StatsModels library v.0.8.0. The cutoff values for differentially expressed gene identification were adjusted such that the P value was smaller than 0.05 (FDR < 0.05) and the absolute value of the log fold change was greater than 1 ($|\log FC| > 1$). Protein–protein interaction (PPI) data with a high confidence value (confidence score >700) were collected from STRING v.10.0.

Adenovirus infection of chondrocytes. Adenoviruses expressing mouse CH25H (Ad-CH25H), CYP7B1 (Ad-CYP7B1), RORα (Ad-RORα), HIF-2α (Ad-HIF-2α), ZIP8 (Ad-ZIP8) and *Cyp7b1* shRNA (Ad-sh*Cyp7b1*) were purchased from Vector Biolabs. Each adenovirus was amplified by infection of HEK-293a cells for 48 h. The HEK cells were harvested and broken by freeze–thaw cycles, and the released adenoviruses were purified by CsCl density gradient ultracentrifugation. Mouse articular chondrocytes were cultured for 3 days, infected with an adenovirus for 2 h at the indicated MOI and cultured for 36 h before further analysis.

Reporter gene assay. Chondrocytes cultured in 96-well plates were transfected with a LightSwitch synthetic Response Elements reporter construct containing the RORE motif (50 ng per well, ActiveMotif), using Lipofectamine RNAiMAX (Invitrogen). After transfection, the cells were treated with IL-1β (1 ng ml^{-1}), TNFα (50 ng ml^{-1}), MβCD-cholesterol (100 μM, Sigma-Aldrich), 25-HC (20 μM, Sigma-Aldrich) or 7α,25-HC (800 nM, Sigma-Aldrich), or infected with 800 MOI of Ad-C, Ad-RORα, Ad-CYP7B1 or Ad-CH25H. The cells were cultured for 36 h before luciferase assay. Renilla luciferase activities were measured using the LightSwitch Luciferase assay reagent.

RNA assay. Total RNA was extracted from primary cultured chondrocytes using the TRI reagent. To isolate RNA from knee joints, mouse and human cartilage tissues were scraped with a blade, and RNA was isolated using the TRI reagent and a Purelink RNA mini kit (Ambion). The RNA was reverse-transcribed, and the resulting cDNA was amplified by PCR (Extended Data Table 1). qRT–PCR was performed in a CFX Connect Real-Time PCR Detection System (Bio-Rad) using SYBR Premix Ex Taq (Tli RNaseH Plus, RR420; TaKaRa Bio). All qRT–PCR reactions were conducted in duplicate, and the amplification signals from individual target genes were normalized to that of glyceraldehyde-3-phosphate dehydrogenase (GAPDH).

Chromatin immunoprecipitation assay. Chromatin immunoprecipitation (ChIP) assays of mouse articular chondrocytes infected with Ad-RORα (800 MOI) were performed using a Magna ChIP A kit (Millipore). In brief, fresh 18.5% paraformaldehyde was applied to the culture medium at a final concentration of 1% to crosslink proteins to DNA. Chromatin was sheared on ice to an average length of 200 to 800 bp with a Vibra-Cell VCX-600 ultrasonic processor (20% amplitude, 9 s pulse on/off, 3 cycles per each sample), and centrifuged at 12,000g. Immunoprecipitation with anti-RORα, washing, and elution were carried out according to the protocol provided with the ChIP kit. Primers for the ChIP assay were designed to amplify RORE-containing promoter regions of the indicated target genes. The RORE motif in each target gene was amplified from immunoprecipitated DNA using the RORα antibody (ChIP) and pre-immunoprecipitated DNA (input). Immunoprecipitated DNA recovered with IgG was used as the negative control.

Western blotting. Total cell lysates were prepared in lysis buffer (150 mM NaCl, 1% NP-40, 50 mM Tris, 5 mM NaF) and used to detect cellular proteins with antibodies purchased from Sigma-Aldrich (RORα), Santa Cruz (SOX9), Millipore (collagen-II) and BD Bioscience (ERK). For detection of secreted proteins (MMP3 and MMP13), 900 μl of serum-free conditioned medium was subjected to trichloroacetic acid (TCA) precipitation and the target proteins were detected using antibodies from Abcam (MMP3) and Aviva Systems Biology (MMP13). All lysis buffers contained a cocktail of protease inhibitors and phosphatase inhibitors.

Binding assay of cholesterol and oxysterols to RORα. Binding of cholesterol, 25-HC and 7α,25-HC to RORα were determined by competition assays performed using fluorescent 22-NBD cholesterol (Thermo Fisher Scientific), which binds to full-length recombinant RORα protein (OriGene). First, saturation fluorescence polarization experiments were performed to examine the binding of 22-NBD cholesterol to RORα. In brief, 200 nM 22-NBD cholesterol was bound with the indicated amounts (nM) of full-length recombinant RORα protein diluted in 25 mM Tris-HCl (pH 7.3), 100 mM glycine and 10% glycerol (v/v). From this assay, we determined the concentration of RORα protein (nM) that gave a consistent fluorescence polarization value. This concentration was fixed, and increasing amounts of cholesterol or its metabolites (25-HC and 7α,25-HC) were added for the competition fluorescence polarization assay. Incubation was carried out in 384-well black flat-bottom plates that had been equilibrated overnight at 4 °C. Polarization was measured using a Molecular Devices FlexStation 3.0 multi-mode microplate reader (Molecular Devices) with λ (ex) = 485 nm and λ (em) = 525 nm, and plotted using the GraphPad Prism 7.00 software. Dissociation constants (K_d) were determined by nonlinear regression analysis of binding saturation and one-site competition curves.

Quantification and statistical analysis. All experiments were performed independently at least four times. Statistical comparisons of two independent groups were made using the Shapiro–Wilk test for normality, Levene's test for homogeneity of variance and the two-tailed independent t-test. Multiple comparisons were performed using the Shapiro–Wilk test, Levene's test and one-way analysis of variance (ANOVA) with post hoc Bonferroni test. Data based on ordinal grading systems were analysed using the non-parametric Mann–Whitney U test. Each n indicates the number of biologically independent samples, mice per group or human specimens. The sample size for each experiment was not predetermined. The P values are indicated in the figures or in Source Data, and the error bars represent s.e.m. for parametric data and the calculated 95% CIs for nonparametric data. Except where stated, the experiments were not randomized and the investigators were not blinded to allocation during experiments and outcome assessment.

Reporting summary. Further information on research design is available in the Nature Research Reporting Summary linked to this paper.

Data availability

Microarray data have been deposited in the Gene Expression Omnibus under accession codes GSE104793 (for IL-1β), GSE104794 (for HIF-2α), and GSE104795 (for ZIP8). Source Data for the Figures and Extended Data Figures are provided in the online version of the paper. Uncropped images of western blots and gels are available in the Supplementary Information.

30. Ryu, J. H. et al. Hypoxia-inducible factor-2α is an essential catabolic regulator of inflammatory rheumatoid arthritis. *PLoS Biol.* **12**, e1001881 (2014).
31. Glasson, S. S., Blanchet, T. J. & Morris, E. A. The surgical destabilization of the medial meniscus (DMM) model of osteoarthritis in the 129/SvEv mouse. *Osteoarthritis Cartilage* **15**, 1061–1069 (2007).
32. Son, Y. O. et al. Estrogen-related receptor γ causes osteoarthritis by upregulating extracellular matrix-degrading enzymes. *Nat. Commun.* **8**, 2133 (2017).
33. Glasson, S. S., Chambers, M. G., Van Den Berg, W. B. & Little, C. B. The OARSI histopathology initiative – recommendations for histological assessments of osteoarthritis in the mouse. *Osteoarthritis Cartilage* **18** (Suppl. 3), S17–S23 (2010).
34. Krenn, V. et al. Synovitis score: discrimination between chronic low-grade and high-grade synovitis. *Histopathology* **49**, 358–364 (2006).
35. Das Neves Borges, P., Vincent, T. L. & Marenzana, M. Automated assessment of bone changes in cross-sectional micro-CT studies of murine experimental osteoarthritis. *PLoS ONE* **12**, e0174294 (2017).
36. Malfait, A. M., Little, C. B. & McDougall, J. J. A commentary on modelling osteoarthritis pain in small animals. *Osteoarthritis Cartilage* **21**, 1316–1326 (2013).
37. Gosset, M., Berenbaum, F., Thirion, S. & Jacques, C. Primary culture and phenotyping of murine chondrocytes. *Nat. Protoc.* **3**, 1253–1260 (2008).
38. Rutkowska, A. *et al.* The EBI2 signalling pathway plays a role in cellular crosstalk between astrocytes and macrophages. *Sci. Rep.* **6**, 25520 (2016).

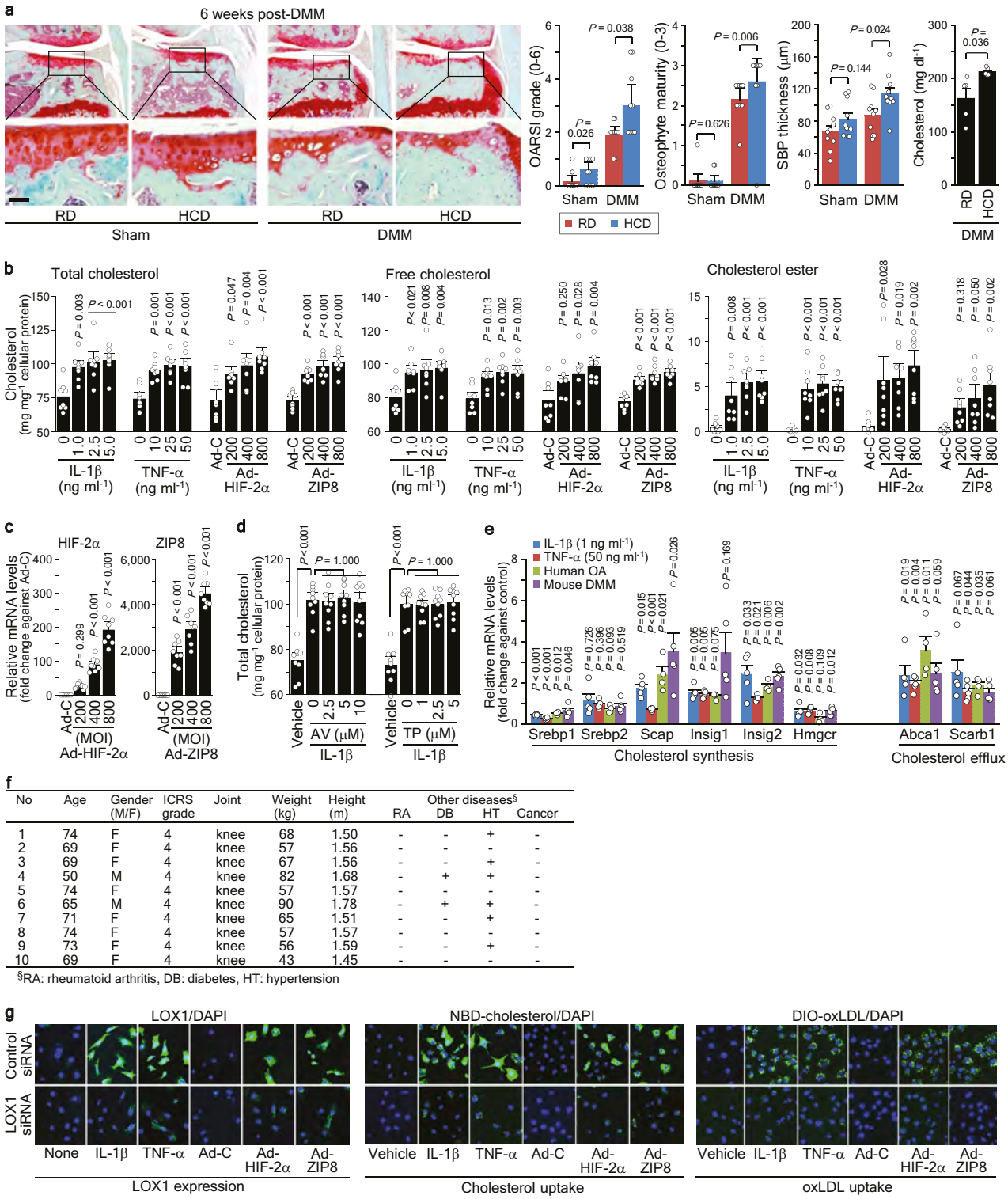

f

No	Age	Gender (M/F)	ICRS grade	Joint	Weight (kg)	Height (m)	Other diseases§ RA	DB	HT	Cancer
1	74	F	4	knee	68	1.50	-	-	+	-
2	69	F	4	knee	57	1.56	-	-	-	-
3	69	F	4	knee	67	1.56	-	-	+	-
4	50	M	4	knee	82	1.68	-	+	+	-
5	74	F	4	knee	57	1.57	-	-	-	-
6	65	M	4	knee	90	1.78	-	+	+	-
7	71	F	4	knee	65	1.51	-	-	+	-
8	74	F	4	knee	57	1.57	-	-	-	-
9	73	F	4	knee	56	1.59	-	-	+	-
10	69	F	4	knee	43	1.45	-	-	-	-

§RA: rheumatoid arthritis, DB: diabetes, HT: hypertension

Extended Data Fig. 1 | See next page for caption.

Extended Data Fig. 1 | OA-associated catabolic signalling increases cholesterol uptake in chondrocytes. a, Mice fed a regular diet (RD) or HCD were subjected to sham operation or DMM surgery. Left to right, safranin-O staining, scoring of cartilage destruction (OARSI grade), osteophyte maturity, subchondral bone plate (SBP) thickness ($n = 10$) and serum cholesterol levels ($n = 5$). **b**, **c**, Cholesterol levels in chondrocytes treated with IL-1β or TNFα for 36 h or infected for 36 h with Ad-C (800 MOI), Ad-HIF-2α or Ad-ZIP8 (**b**). Levels of *Hif2a* (also known as *Epas1*) and *Zip8* (also known as *Slc39a8*) mRNA in adenovirus-infected chondrocytes (**c**). $n = 8$ each. **d**, Cholesterol levels in chondrocytes treated with IL-1β (5 ng ml^{-1}) and the cholesterol synthesis inhibitors triparanol (TP) or atorvastatin (AV) for 36 h ($n = 9$). **e**, mRNA levels of proteins involved in cholesterol synthesis and efflux in chondrocytes treated with IL-1β or TNFα ($n = 5$) or in damaged regions of human OA (versus undamaged regions, $n = 4$) and DMM-operated cartilage (versus sham operation, $n = 5$). **f**, Characteristics of individuals with OA from whom cartilage samples were taken. **g**, Representative images ($n = 5$) of LOX1 expression, NBD-cholesterol uptake, and DIO-oxLDL uptake in chondrocytes treated with control or *Lox1* siRNA with or without IL-1β or TNFα, or infected with 800 MOI of Ad-C, Ad-HIF-2α or Ad-ZIP8. Means ± 95% CI with Mann–Whitney *U* test for OARSI grade and osteophyte maturity; means ± s.e.m. with two-tailed *t*-test for SBP thickness and cholesterol levels (**a**). Means ± s.e.m. with one-way ANOVA and Bonferroni test (**b**, **c**, **d**) and means ± s.e.m. with two-tailed *t*-test (**e**). *n* indicates the number of biologically independent samples or mice per group. Exact *P* values (for $P < 0.001$) can be found in the accompanying Source Data. Scale bar, 25 μm.

a

Category	Gene symbol	IL-1β (1 ng ml^{-1}, 36h)	Ad-HIF-2α (800 MOI, 36h)	Ad-ZIP8 (800 MOI, 36h)
Cholesterol efflux	*Abca1*	2.81 ± 0.19	2.55 ± 0.16	2.35 ± 0.20
	Abcg1	1.01 ± 0.22	1.41 ± 0.26	1.26 ± 0.25
	Apoa1	0.87 ± 0.23	1.08 ± 0.14	1.03 ± 0.23
	Apoe	1.08 ± 0.18	1.04 ± 0.13	1.11 ± 0.19
	Pparg	1.03 ± 0.21	0.90 ± 0.22	0.95 ± 0.23
Cholesterol influx	*Msr1*	1.01 ± 0.35	1.03 ± 0.41	0.98 ± 0.42
	Cd36	1.00 ± 0.26	1.00 ± 0.24	1.00 ± 0.24
	Olr1	0.96 ± 0.18	1.02 ± 0.30	0.98 ± 0.34
	Scarb1	2.06 ± 0.12	2.11 ± 0.13	1.57 ± 0.11
	Apob	1.05 ± 0.24	1.04 ± 0.21	1.14 ± 0.36
	Mylip	1.51 ± 0.17	1.14 ± 0.26	1.21 ± 0.27
	Ldlr	1.03 ± 0.12	0.96 ± 0.15	0.95 ± 0.11
	Vldlr	1.54 ± 0.22	0.98 ± 0.15	0.96 ± 0.13
Cholesterol synthesis	*Srebf1*	0.90 ± 0.20	0.97 ± 0.14	0.97 ± 0.12
	Srebf2	1.18 ± 0.05	1.04 ± 0.13	1.00 ± 0.11
	Hmgcr	0.99 ± 0.06	1.01 ± 0.08	0.99 ± 0.12
	Hmgcs1	1.86 ± 0.12	1.16 ± 0.09	1.00 ± 0.07
	Hmgcs2	0.76 ± 0.35	0.82 ± 0.29	0.93 ± 0.22
	Dhcr7	1.26 ± 0.13	0.91 ± 0.22	0.96 ± 0.23
Cholesterol hydroxylase	*Ch25h*	30.69 ± 0.29	4.58 ± 0.33	3.91 ± 0.47
	Cyp3a11	1.01 ± 0.35	1.02 ± 0.23	1.00 ± 0.25
	Cyp7a1	0.94 ± 0.25	0.92 ± 0.24	1.09 ± 0.24
	Cyp7b1	9.33 ± 0.46	4.64 ± 0.24	4.24 ± 0.26
	Cyp8b1	0.93 ± 0.24	1.01 ± 0.37	0.84 ± 0.40
	Cyp27a1	0.76 ± 0.39	0.67 ± 0.25	0.67 ± 0.29
	Cyp39a1	0.55 ± 0.36	0.79 ± 0.28	0.98 ± 0.16
	Cyp46a1	0.95 ± 0.12	0.89 ± 0.11	1.02 ± 0.11
Cholesterol dehydrogenase	*Hsd3b7*	1.19 ± 0.07	1.23 ± 0.27	1.11 ± 0.25
Oxysterol receptors	*Nr1f1*	1.98 ± 0.26	1.40 ± 0.14	1.34 ± 0.16
	Nr1f3	0.72 ± 0.12	0.69 ± 0.29	0.80 ± 0.22
	Nr1h2	1.39 ± 0.03	1.14 ± 0.16	1.10 ± 0.17
	Nr1h3	1.27 ± 0.16	1.41 ± 0.18	1.52 ± 0.16
	Nr1h4	1.00 ± 0.21	0.99 ± 0.21	0.99 ± 0.17
	Gpr183	1.03 ± 0.48	0.97 ± 0.25	0.86 ± 0.42
	Cxcr2	1.04 ± 0.22	0.96 ± 0.30	0.91 ± 0.31
	Esr1	0.87 ± 0.19	1.02 ± 0.19	1.14 ± 0.20

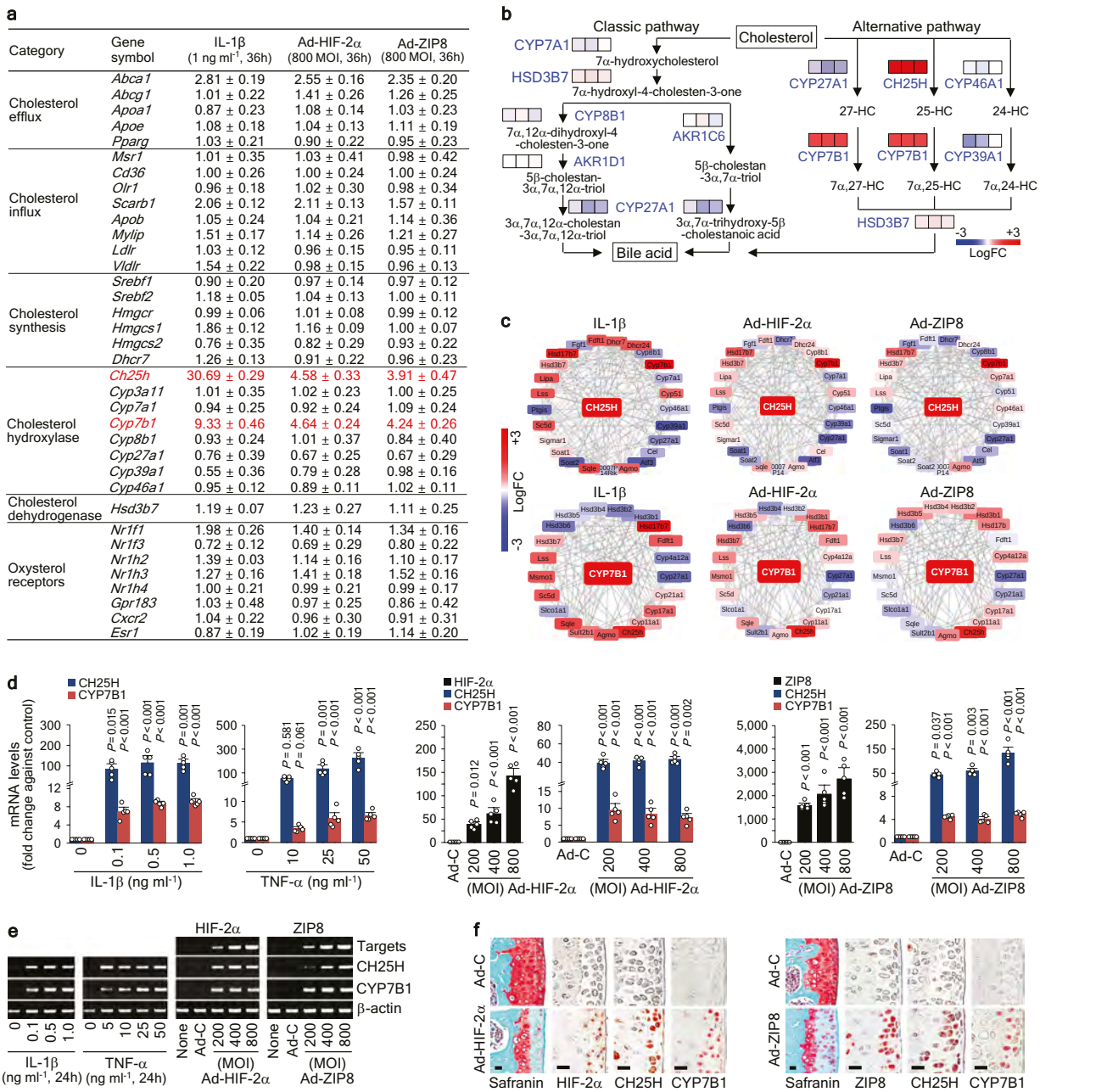

Extended Data Fig. 2 | Upregulation of CH25H and CYP7B1 in OA chondrocytes. a–c, Microarray analysis of cholesterol metabolism-related genes in chondrocytes treated with IL-1β, Ad-C (control), Ad-HIF-2α or Ad-ZIP8. **a**, Fold changes in mRNA levels versus those in vehicle or Ad-C-infected cells ($n = 4$). **b**, Heat maps (left, IL-1β; centre, Ad-HIF-2α; right, Ad-ZIP8) of genes involved in cholesterol metabolism and metabolic pathways of bile acid synthesis in the liver. **c**, PPI network based on CH25H and CYP7B1. Nodes and links represent protein-encoding genes and their interactions, respectively. Genes shown in red and blue indicate those annotated as upregulated and downregulated, respectively, in the PPI network. **d**, **e**, mRNA levels (**d**) and representative RT–PCR gel images (**e**) in chondrocytes treated with IL-1β or TNFα, or infected with Ad-C (800 MOI; left), Ad-HIF-2α (middle) or Ad-ZIP8 (right; $n = 5$). **f**, Safranin-O staining and immunostaining of the indicated proteins in mice that underwent intra-articular injection of Ad-HIF-2α or Ad-ZIP8 ($n = 7$). Means ± s.e.m. with one-way ANOVA and Bonferroni test. *n* indicates the number of biologically independent samples or mice per group. Exact *P* values (for $P < 0.001$) can be found in the accompanying Source Data. For gel source data, see Supplementary Fig. 1. Scale bars, 25 μm.

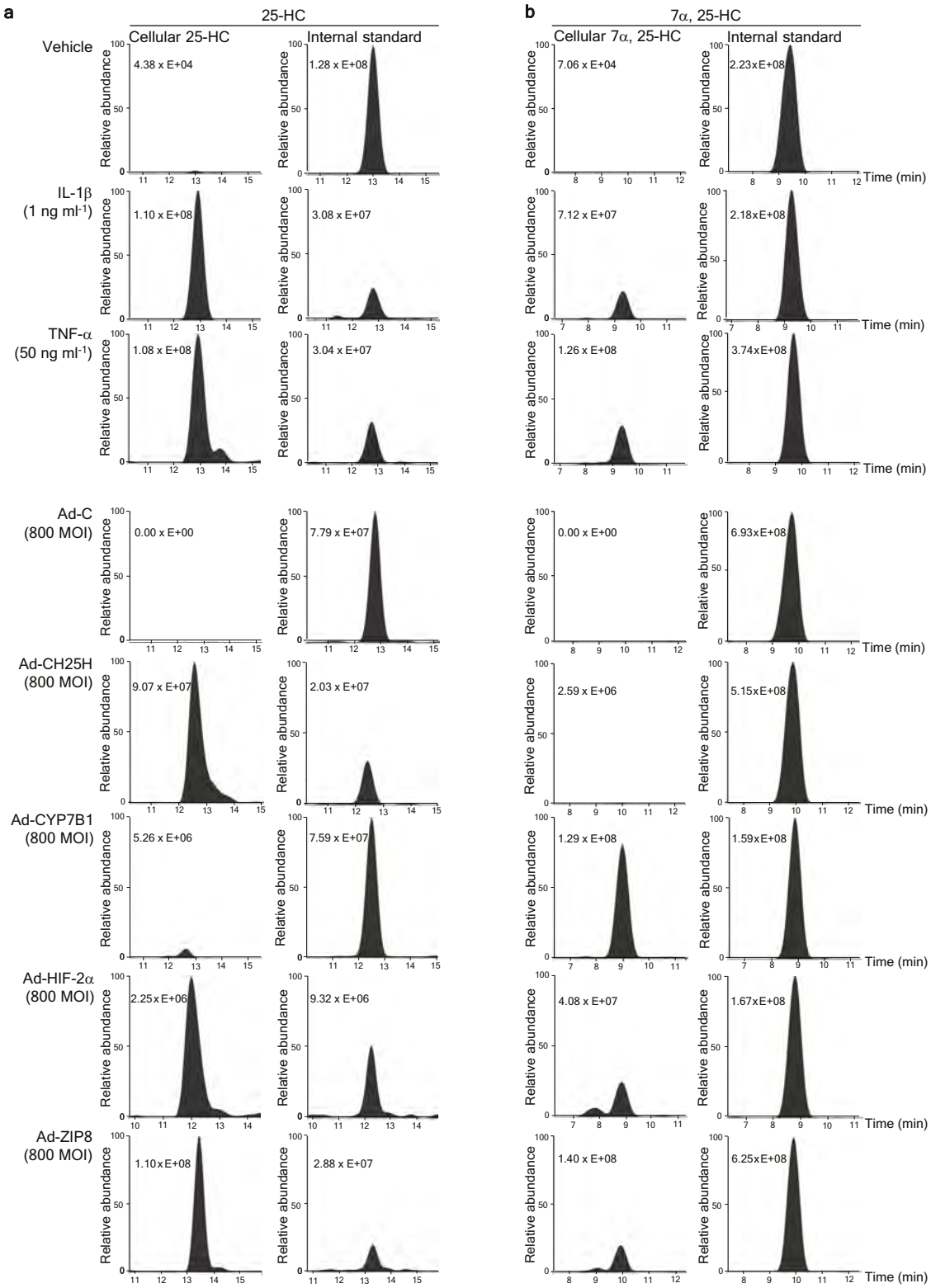

Extended Data Fig. 3 | Production of oxysterols in chondrocytes stimulated with OA-associated catabolic signalling. a, **b**, Chondrocytes were treated with IL-1β or TNFα, or infected with 800 MOI of Ad-C, Ad-CH25H, Ad-CYP7B1, Ad-HIF-2α or Ad-ZIP8. The amounts of 25-HC (**a**) and 7α,25-HC (**b**) were measured using HPLC–MS/MS ($n = 4$ biologically independent samples). Representative peak areas of endogenous oxysterols and corresponding internal standards are shown.

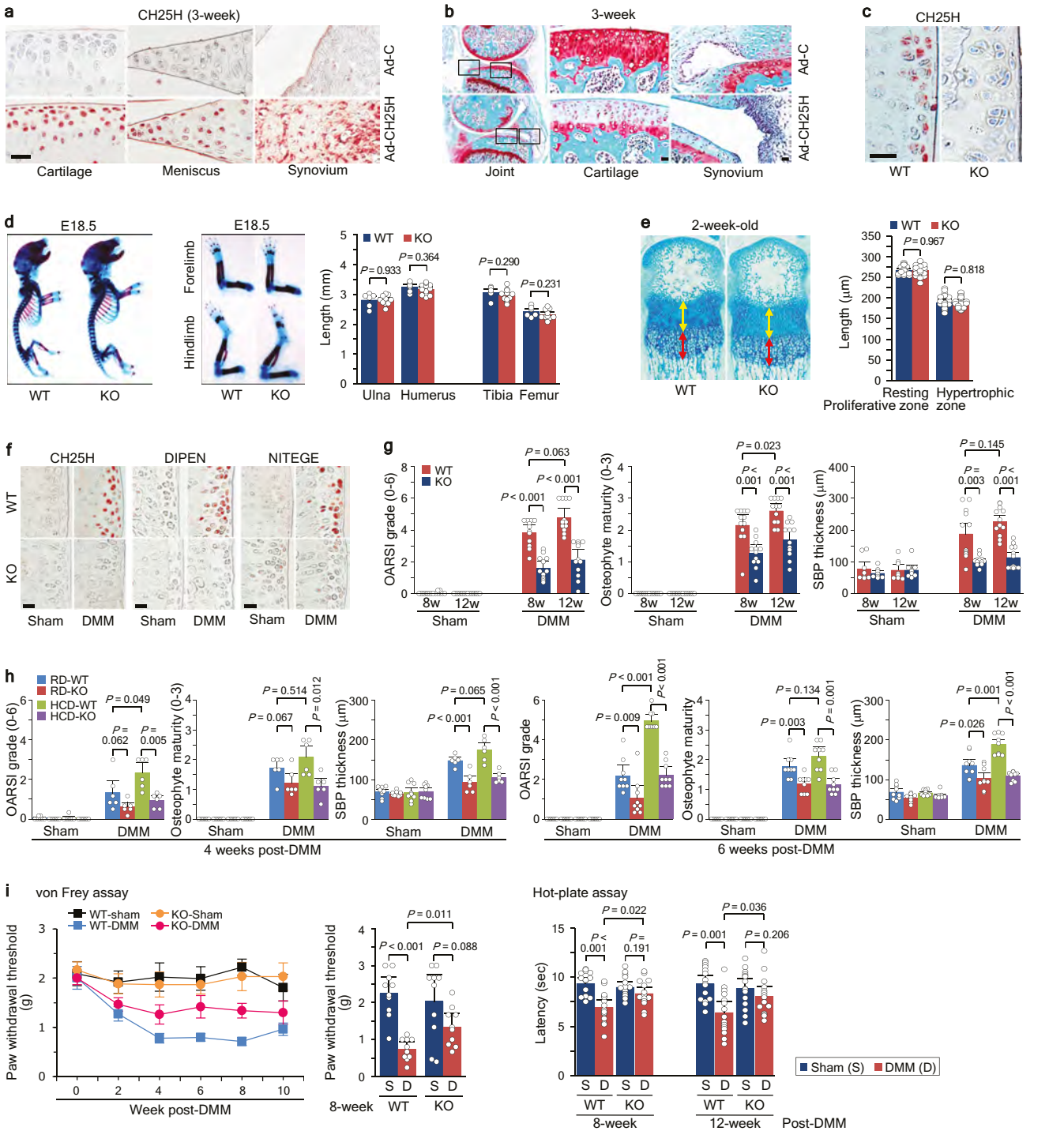

Extended Data Fig. 4 | CH25H regulates OA pathogenesis in mice. **a**, **b**, Representative images of CH25H immunostaining (**a**) and safranin-O staining (**b**) in mice that underwent intra-articular injection of Ad-C or Ad-CH25H once weekly for 3 weeks ($n = 12$ mice per group). **c**, Representative immunostaining of CH25H in cartilage sections of 20-week-old wild-type and *Ch25h*$^{-/-}$ (KO) mice ($n = 12$ per group). **d**, Staining of whole skeleton, hindlimbs and forelimbs, and the length of the indicated bones, in wild-type ($n = 6$) and *Ch25h*$^{-/-}$ ($n = 12$) mice. **e**, Staining of growth plates in metatarsal bones, along with the lengths of the indicated zones, from *Ch25h*$^{-/-}$ mice and wild-type littermates ($n = 20$ mice per group). **f**, Representative immunostaining images of CH25H, DIPEN and NITEGE in *Ch25h*$^{-/-}$ and wild-type littermates subjected to sham or DMM surgery ($n = 8$ mice per group). **g**, OA parameters quantified 8 and 12 weeks after *Ch25h*$^{-/-}$ and wild-type littermates were subjected to sham operation ($n = 8$ mice) or DMM surgery ($n = 12$ mice). **h**, Wild-type and *Ch25h*$^{-/-}$ mice fed regular diet or HCD were subjected to sham or DMM operations, with OA parameters quantified at 4 ($n = 8$ mice for sham and 6 mice for DMM) and 6 weeks ($n = 9$ mice for sham and 9 mice for DMM). **i**, von Frey ($n = 10$ mice per group) and hot-plate ($n = 15$ mice per group) pain assays in DMM-operated *Ch25h*$^{-/-}$ and wild-type mice at the indicated times after operation. Means ± s.e.m. with two-tailed *t*-test (**d**, **e**). Means ± 95% CI with Mann–Whitney *U* test for OARSI grade, osteophyte maturity and von Frey assay; means ± s.e.m. with two-tailed *t*-test for SBP thickness and hot-plate assay (**g**–**i**). Exact *P* values (for $P < 0.001$) can be found in the accompanying Source Data. Scale bars, 25 μm.

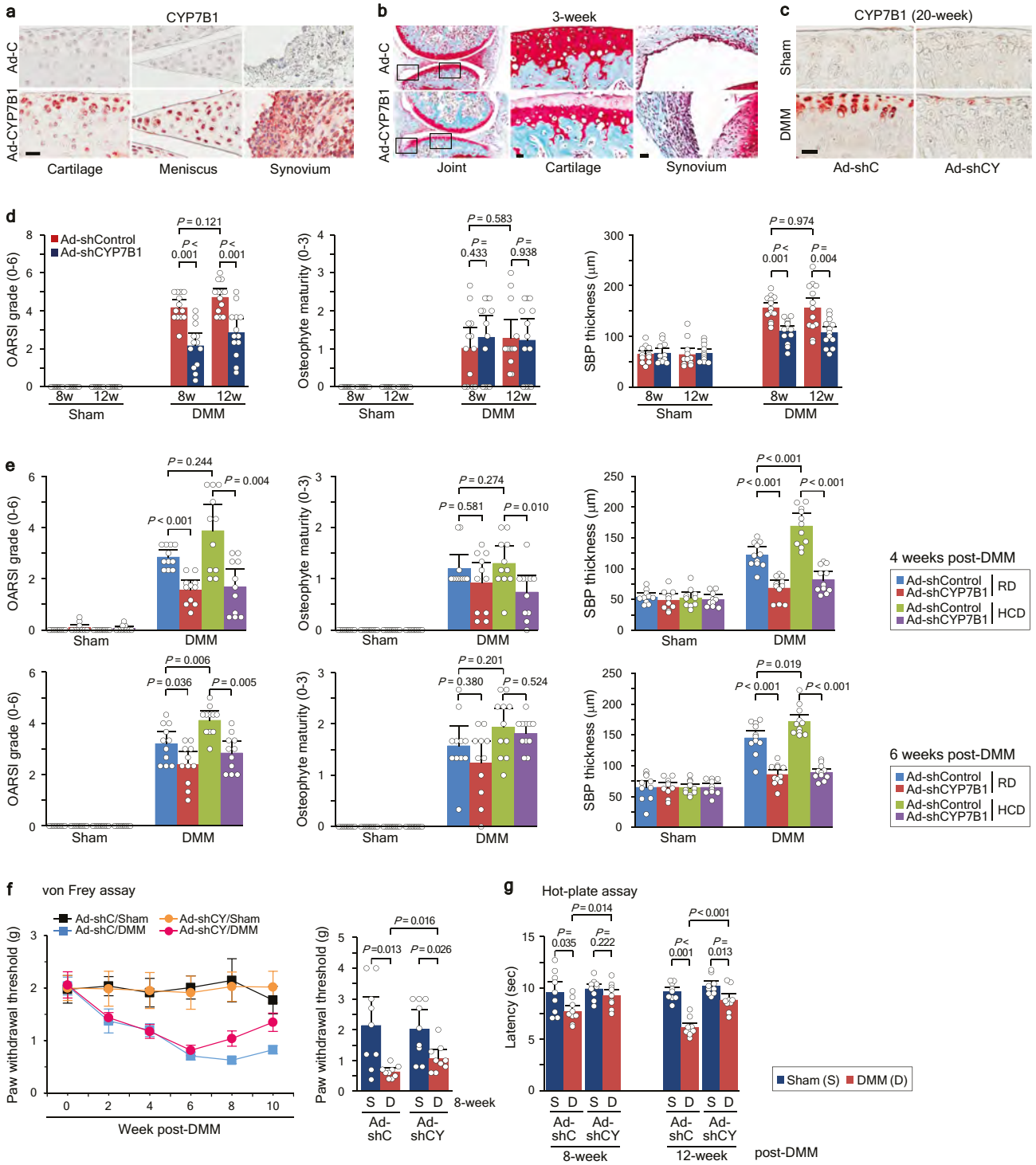

Extended Data Fig. 5 | CYP7B1 regulates OA pathogenesis in mice. **a**, **b**, Wild-type mice underwent intra-articular injection of Ad-C or Ad-CYP7B1 and were killed three weeks later. Representative images of CYP7B1 immunostaining (**a**) and safranin-O staining (**b**). $n = 9$ mice per group. **c**, **d**, Sham- or DMM-operated mice underwent intra-articular injection of Ad-shControl or Ad-sh*Cyp7b1*, and were killed 8 or 12 weeks later. Representative immunostaining images of CYP7B1 in cartilage sections (**c**) and quantification of OA parameters (**d**). $n = 10$ mice for sham and 13 mice for DMM. **e**, Sham- or DMM-operated mice fed regular diet or HCD underwent intra-articular injection of Ad-shControl or Ad-sh*Cyp7b1*. The mice were killed four or six weeks after the operation, and OA parameters were quantified ($n = 10$ mice for sham and 11 mice for DMM). **f**, **g**, Pain assays. Sham- or DMM-operated mice underwent intra-articular injection of Ad-shControl or Ad-sh*Cyp7b1* ($n = 9$ mice per group) and were subjected to von Frey (**f**) and hot-plate (**g**) assays. Means ± 95% CI with Mann–Whitney *U* test for OARSI grade, osteophyte maturity and von Frey assay; means ± s.e.m. with two-tailed *t*-test for SBP thickness and hot-plate assay (**d**–**g**). Exact *P* values (for $P < 0.001$) can be found in the accompanying Source Data. Scale bars, 25 μm.

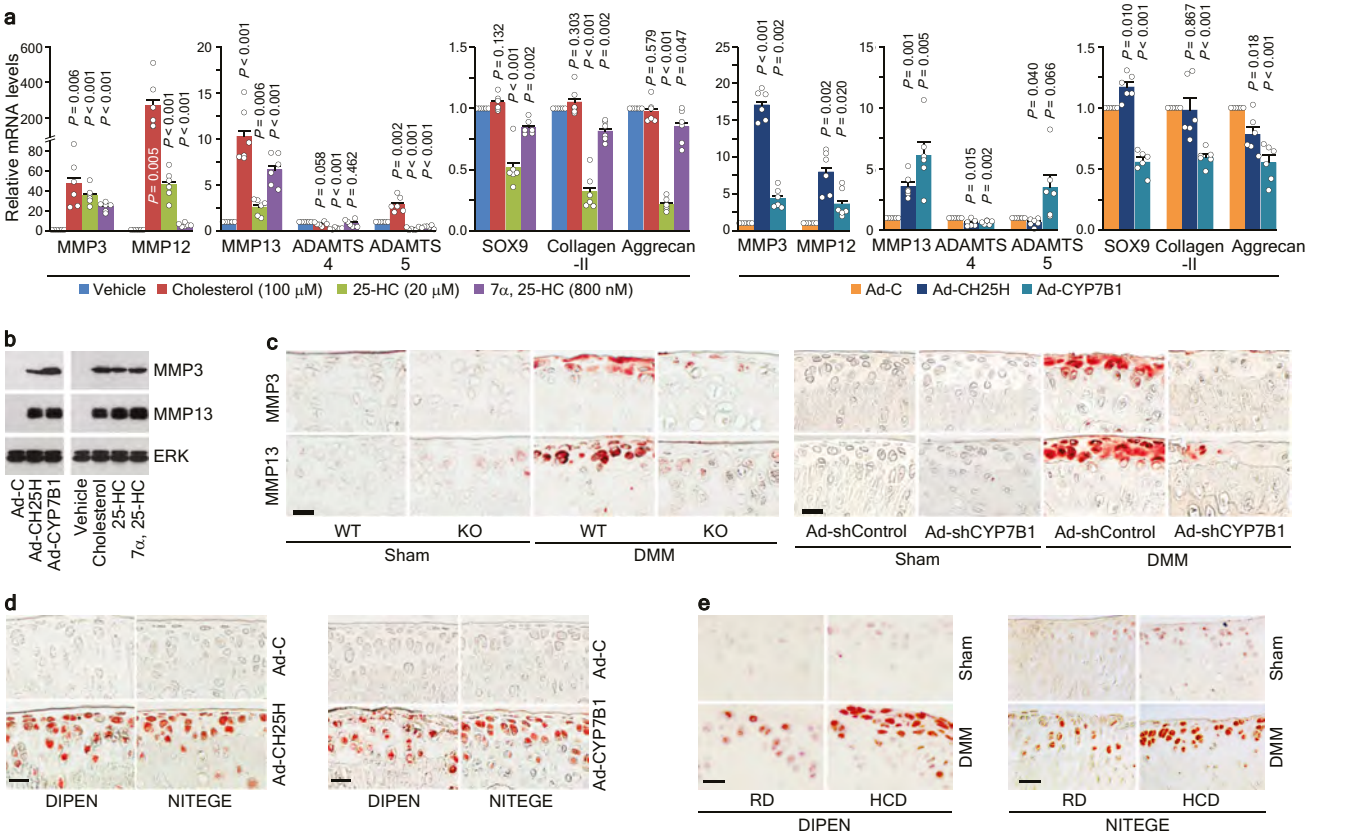

Extended Data Fig. 6 | Cholesterol metabolism regulates the expression of matrix-degrading enzymes in chondrocytes. a, **b**, Mouse articular chondrocytes in primary culture were treated for 36 h with MβCD-cholesterol, 25-HC or 7α,25-HC. Alternatively, chondrocytes were infected with 800 MOI of Ad-C, Ad-CH25H or Ad-CYP7B1. **a**, Relative mRNA levels (fold change against control) of the indicated molecules were quantified by qRT–PCR analysis ($n = 6$ biologically independent samples). **b**, Western blots of secreted MMP3 and MMP13 in the culture supernatants of chondrocytes ($n = 5$ biologically independent samples). **c**, Representative immunostaining of MMP3 and MMP13 in cartilage from sham- or DMM-operated wild-type and *Ch25h*$^{-/-}$ mice (left) and DMM-operated wild-type mice that received intra-articular injection of Ad-shControl or Ad-sh*Cyp7b1* (right; $n = 8$ mice per group). **d**, **e**, Detection of aggrecan neoepitopes in the cartilage of mice that received intra-articular injection of Ad-C, Ad-CH25H or Ad-CYP7B1 (**d**; $n = 8$ mice per group) and sham- or DMM-operated mice fed regular diet or HCD (**e**, $n = 10$ mice per group). Means ± s.e.m. with two-tailed *t*-test. Exact *P* values (for $P < 0.001$) can be found in the accompanying Source Data. Scale bars, 25 μm.

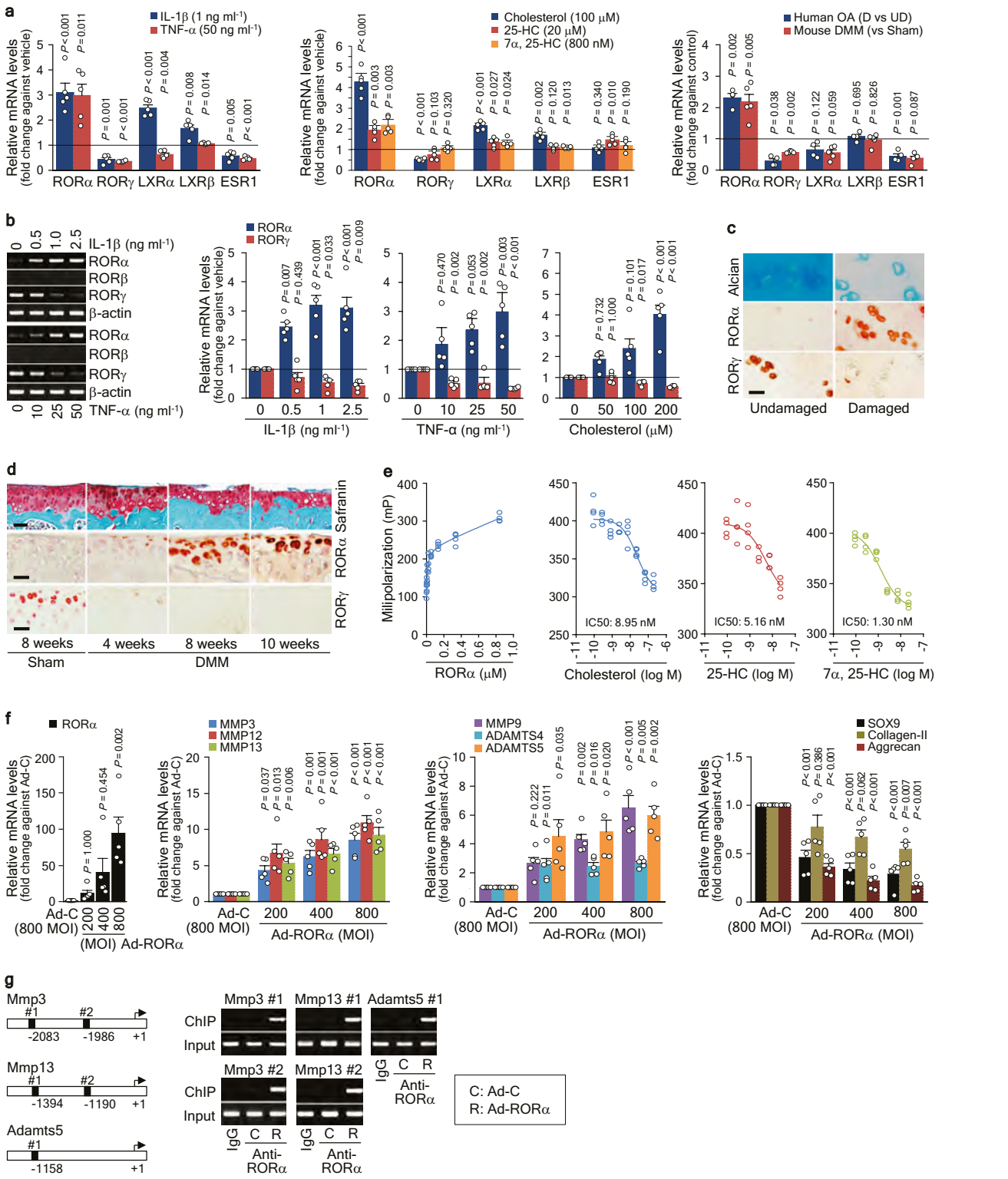

Extended Data Fig. 7 | RORα is a downstream mediator of cholesterol metabolism in chondrocytes. a, mRNA levels of putative oxysterol-binding nuclear receptors in chondrocytes treated with IL-1β, TNFα, cholesterol, 25-HC or 7α,25-HC for 36 h ($n = 5$), in damaged regions of cartilage from humans with OA (versus undamaged regions; $n = 4$), and in cartilage from DMM-operated mice (versus sham-operated mice; $n = 5$). **b**, RT–PCR and qRT–PCR ($n = 5$) analyses of ROR isoforms in chondrocytes treated with IL-1β or TNFα for 36 h. **c**, **d**, Representative immunostaining images of RORα and RORγ in damaged and undamaged regions of cartilage from the same patient (**c**; $n = 10$) and sham- or DMM-operated mice (**d**; $n = 7$). **e**, Left, saturation fluorescent polarization assays assessing the binding of 22-NBD cholesterol (200 nM) to increasing amounts of full-length recombinant RORα protein. Right, competition fluorescent polarization assays to determine the competition of the indicated concentrations of cholesterol, 25-HC, and 7α,25-HC with 22-NBD cholesterol (200 nM) for binding to full-length recombinant RORα protein (5 nM; $n = 4$). **f**, qRT–PCR analysis of the indicated molecules in chondrocytes infected with Ad-RORα ($n = 5$). **g**, ChIP assays for RORα binding to the promoter of each target gene in chondrocytes infected with 800 MOI of Ad-C (C) or Ad-RORα (R) ($n = 5$). Means ± s.e.m. with two-tailed *t*-test (**a**) and with one-way ANOVA and Bonferroni test (**b**, **f**). *n* indicates the number of biologically independent samples, mice per group, or human specimens. Exact *P* values (for $P < 0.001$) can be found in the accompanying Source Data. For gel source data, see Supplementary Fig. 1. Scale bars, 25 μm.

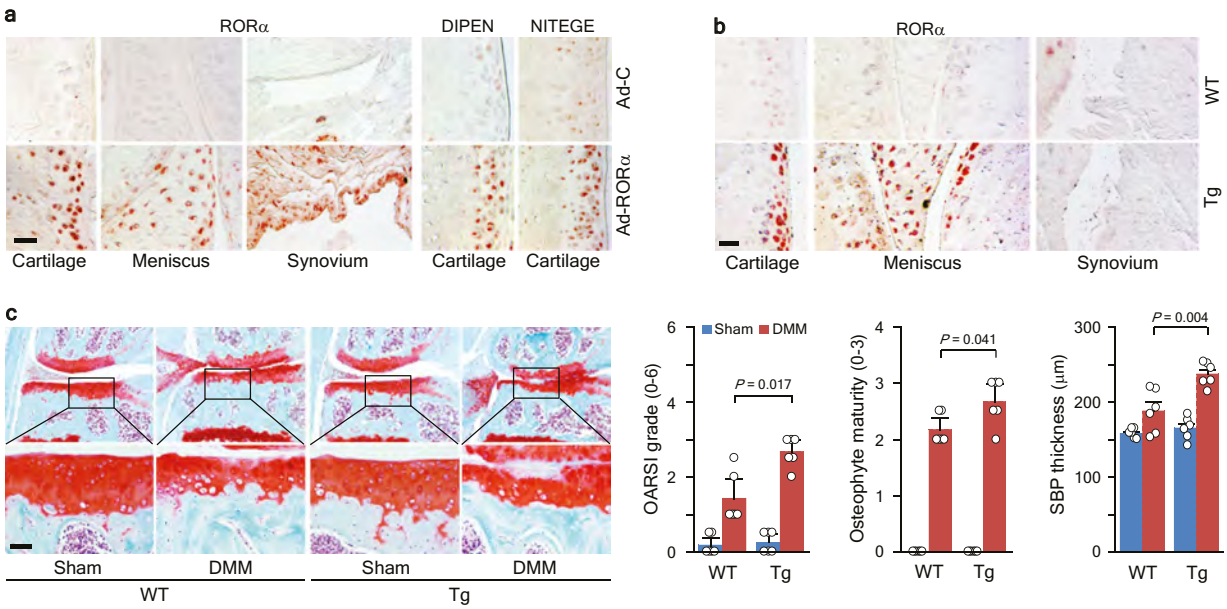

Extended Data Fig. 8 | RORα overexpression enhances experimental OA in mice. a, Representative immunostaining images of RORα and the aggrecan neoepitopes DIPEN and NITEGE in cartilage of mice that received intra-articular injection of Ad-C or Ad-RORα ($n = 5$ mice per group). **b**, Representative immunostaining images of RORα in knee joint sections of transgenic and wild-type mice ($n = 4$ mice each). **c**, Transgenic and wild-type mice were subjected to sham operation or DMM surgery. Representative safranin-O staining images of joint sections (left) and quantification of OARSI grade, osteophyte maturity and SBP thickness (right; $n = 6$ mice per group), 6 weeks after sham operation or DMM surgery. Means ± 95% CI with Mann–Whitney *U* test for OARSI grade and osteophyte maturity; means ± s.e.m. with two-tailed *t*-test for SBP thickness. Exact *P* values (for $P < 0.001$) can be found in the accompanying Source Data. Scale bars, 25 μm.

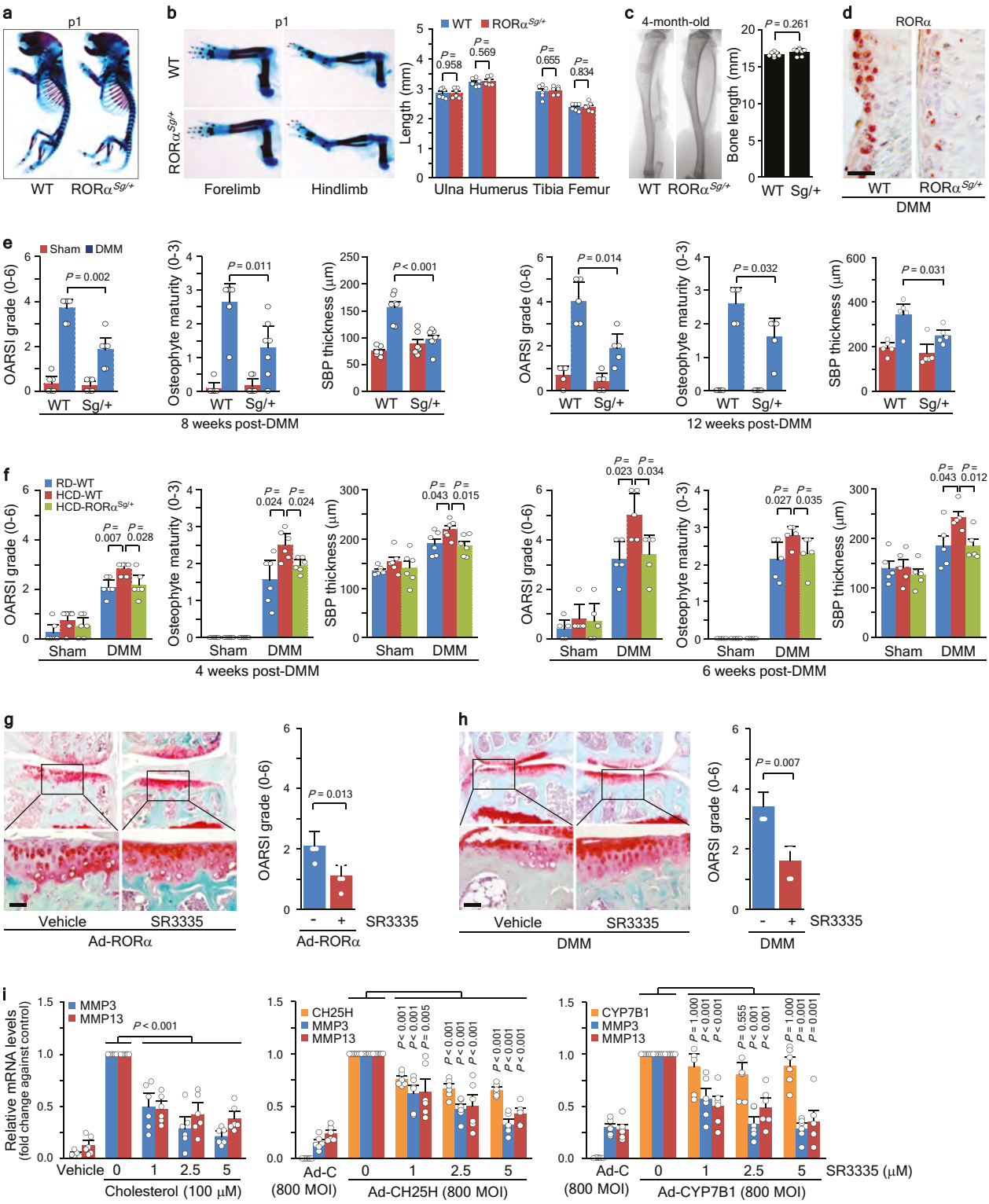

Extended Data Fig. 9 | Regulation of OA pathogenesis by RORα. **a**–**c**, Whole-skeleton staining (**a**), staining of hindlimbs and forelimbs and lengths of the indicated bones on postnatal day 1 in *Rora*$^{Sg/+}$ and wild-type mice (**b**; $n = 6$ each), and representative microCT images of the tibia and the length of the indicated region in 4-month-old *Rora*$^{Sg/+}$ and wild-type mice (**c**; $n = 8$ each). **d**, Representative immunostaining images of RORα in cartilage sections from DMM-operated *Rora*$^{Sg/+}$ and wild-type mice ($n = 5$ each). **e**, Quantification of OA manifestations 8 ($n = 6$ mice for sham and 7 mice for DMM) or 12 ($n = 5$ each) weeks after sham or DMM surgery in *Rora*$^{Sg/+}$ and wild-type mice. **f**, *Rora*$^{Sg/+}$ and wild-type mice fed regular diet or HCD were subjected to sham or DMM surgery, and OA parameters were quantified after 4 ($n = 6$ each) or 6 ($n = 5$ each) weeks. **g**, **h**, Safranin-O staining and scoring of OARSI grade in mice that underwent intra-articular injection of Ad-RORα with vehicle or SR3335, or sham- or DMM-operated mice that underwent intra-articular injection of vehicle or SR3335 ($n = 5$ mice each). **i**, mRNA levels of indicated molecules in chondrocytes treated with cholesterol for 36 h or infected with Ad-C, Ad-CH25H or Ad-CYP7B1 for 36 h in the presence of the indicated concentrations of SR3335 ($n = 6$ mice per group). Means ± s.e.m. with two-tailed *t*-test (**b**, **c**). Means ± 95% CI with Mann–Whitney *U* test for OARSI grade and osteophyte maturity; means ± s.e.m. with two-tailed *t*-test for SBP thickness (**e**–**h**). Means ± s.e.m. with one-way ANOVA and Bonferroni test (**i**). Exact *P* values (for $P < 0.001$) can be found in the accompanying Source Data. Scale bars, 25 μm.

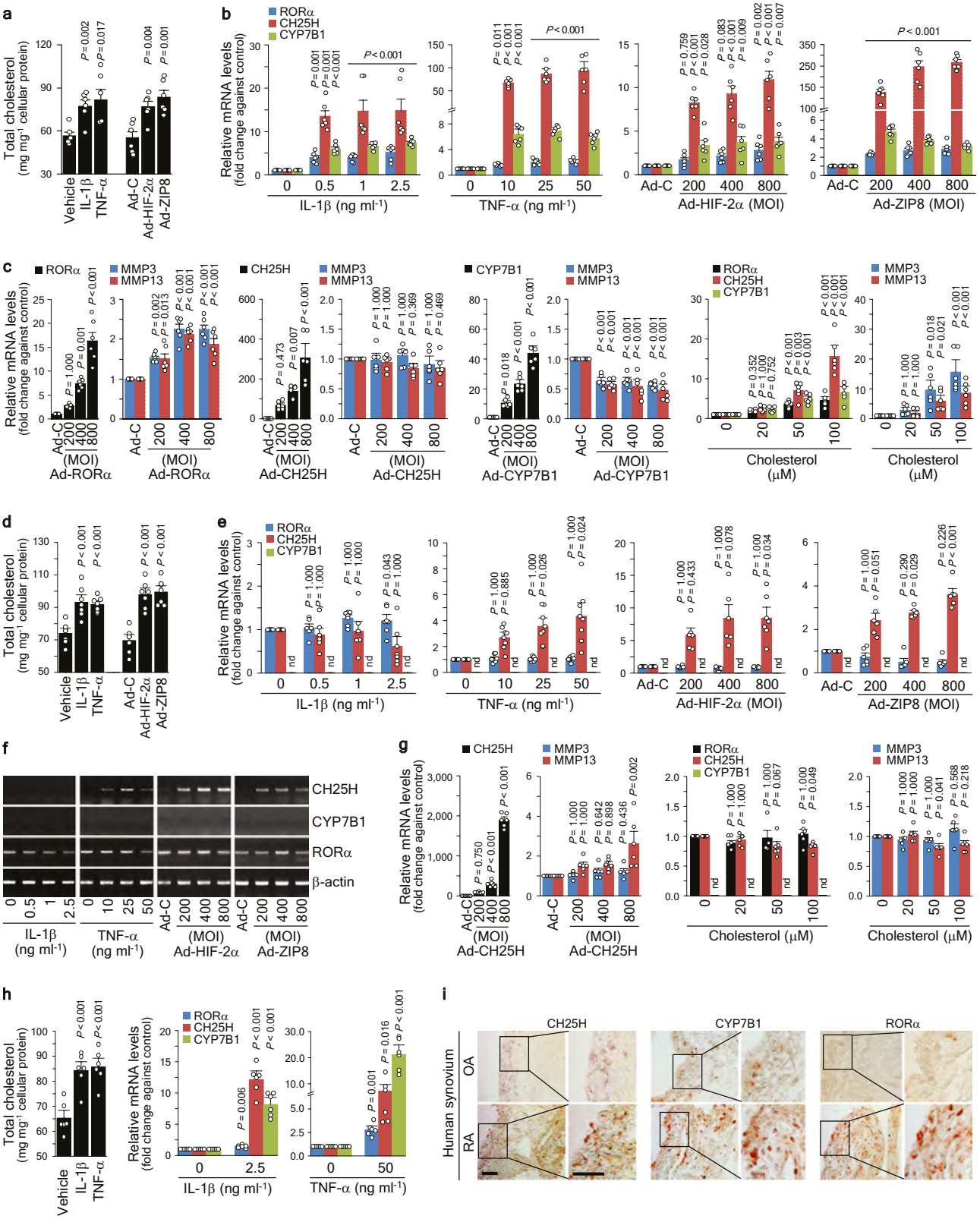

Extended Data Fig. 10 | See next page for caption.

Extended Data Fig. 10 | Regulation of cholesterol metabolism by OA-associated catabolic signalling in FLSs and Raw264.7 cells. a, Total cholesterol levels in FLSs treated with IL-1β (1 ng ml^{-1}, 36 h) or TNFα (50 ng ml^{-1}, 36 h) or infected with 800 MOI of Ad-C, Ad-HIF-2α or Ad-ZIP8 for 36 h ($n = 6$). **b**, mRNA levels in FLSs treated with IL-1β or TNFα or infected with Ad-HIF-2α or Ad-ZIP8 ($n = 6$). **c**, mRNA levels of the indicated molecules in FLSs treated with cholesterol or infected with Ad-CH25H, Ad-CYP7B1 or Ad-RORα ($n = 6$). **d**, Total cholesterol levels in Raw264.7 cells treated as in **a** ($n = 7$). **e**, mRNA levels of the indicated molecules in Raw264.7 cells treated with IL-1β or TNFα or infected with Ad-C, Ad-HIF-2α or Ad-ZIP8 ($n = 7$). **f**, RT–PCR analysis of the indicated molecules in Raw264.7 cells treated with IL-1β or TNFα or infected with Ad-HIF-2α or Ad-ZIP8 ($n = 7$). **g**, mRNA levels in Raw264.7 cells treated with cholesterol or infected with Ad-CH25H ($n = 6$). **h**, Total cholesterol levels and mRNA levels ($n = 6$) of the indicated molecules in human normal chondrocytes treated with IL-1β (2.5 ng ml^{-1}, 36 h) or TNFα (50 ng ml^{-1}, 36 h). **i**, Representative immunostaining images of CH25H, CYP7B1 and RORα in synovial tissue from humans with OA or rheumatoid arthritis ($n = 4$). Means ± s.e.m. with two-tailed *t*-test (**a**, **d**, **h**) or with one-way ANOVA and Bonferroni test (**b**, **c**, **e**, **g**). *n* indicates the number of biologically independent samples or human specimens. Exact *P* values (for $P < 0.001$) can be found in the accompanying Source Data. For gel source data, see Supplementary Fig. 1. Scale bars, 25 μm.

Extended Data Table 1 | Sequences of primers, shRNA and siRNA

Targets	Sequences	Purpose	Targets	Sequences	Purpose
ABCA1 (mouse)	S 5′GTCAGCTCTCAGGTGGGATG3′ AS 5′CGATGGTCAGCGTGTCACTT3′	RT-PCR	ABCA1 (human)	S 5′GCGACCATGAGAGTGACACG3′ AS 5′GCATCCACCCCACTCTCTTC3′	RT-PCR
ADAMTS4 (mouse)	S 5′CATCCGAAACCCTGTCAACTTG3′ AS 5′GCCCATCATCTTCCACAATAGC3′	RT-PCR	ADAMTS5 (mouse)	S 5′GCCATTGTAATAACCCTGCACC3′ AS 5′TCAGTCCCATCCGTAACCTTTG3′	RT-PCR
ADAMTS5 ChIP #1 (mouse)	S 5′TGTAAGTGTGCCTGCTCTCCTCT3′ AS 5′CCTCCATCCTTTGTTTCCTCTAAT3′	CHiP	Aggrecan (mouse) (1)	S 5′CTGTCTTTGTCACCCACACAT3′ AS 5′GAAGACGACATCACCATCCAG3′	RT-PCR
Aggrecan (mouse) (2)	S 5′GAAGACGACATCACCATCCAG3′ AS 5′CTGTCTTTGTCACCCACACATG3′	RT-PCR	β-Actin (mouse) (1)	S 5′ATATCGCTGCGCTGGTCGTC3′ AS 5′AGGATGGCGTGAGGGAGAGC3′	RT-PCR
β-Actin (mouse) (2)	S 5′AGGGTGTGATGGTGGGAATGGGTC3′ AS 5′ACGACCAGAGGCATACAGGGACAG3′	RT-PCR	β-Actin (human)	S 5′GAAGGATTCCTATGTGGGCG3′ AS 5′GATAGCACAGCCTGGATAGCA3′	RT-PCR
COL2A1 (mouse)	S 5′CACACTGGTAAGTGGGGCAAGACCG3′ AS 5′GGATTGTGTTGTTTCAGGGTTCGGG3′	RT-PCR	CH25H (mouse)	S 5′GTGCTGGACGTCCTGTATCC3′ AS 5′AGCACGTCGAAGAAGGTCAG3′	RT-PCR
CH25H (human)	S 5′GGTCATCTTCTCCATCACCACA3′ AS 5′TCCATGTCGAAGAGTAGCAGG3′	RT-PCR	CYP7B1 (mouse)	S 5′GTGCGAAAGGGAGACTTGGT3′ AS 5′AGCGGCTGTAGTTTAGTCCT3′	RT-PCR
CYP7B1 (human)	S 5′TCTCTTTGCCGCCACCTTAC3′ AS 5′AGGCTTTCGCTGATAATCGG3′	RT-PCR	ESR1 (mouse)	S 5′AAAGGCGGCATACGGAAAGA3′ AS 5′TAGATCATGGGCGGTTCAGC3′	RT-PCR
ESR1 (human)	S 5′AGACATGAGAGCTGCCAACC3′ AS 5′AGGATCTCTAGCCAGGCACA3′	RT-PCR	GAPDH (human)	S 5′CGTCTTCACCACCATGGAGA3′ AS 5′CGGCCATCACGCCACAGTTT3′	RT-PCR
GAPDH (mouse)	S 5′TCACTGCCACCCAGAAGAC3′ AS 5′TGTAGGCCATGAGGTCCAC3′	RT-PCR	HIF-2α (mouse)	S 5′CGAGAAGAACGACGTGGTGTTC3′ AS 5′GTGAAGGCTGGCAGGCTCC3′	RT-PCR
HMGCR (mouse)	S 5′GGCCCCACATTCACTCTTGA3′ AS 5′ATCCAGCGACTATGAGCGTG3′	RT-PCR	HMGCR (human)	S 5′TTGGTGATGGGAGCTTGTTGT3′ AS 5′CGAGCCAGGCTTTCACTTCT3′	RT-PCR
INSIG1 (mouse)	S 5′TCTCATTTGGCGTGGTCCTG3′ AS 5′CTAATTTGGCACTGGCGTGG3′	RT-PCR	INSIG1 (human)	S 5′CATCTTTTCCTCCGCCTGGT3′ AS 5′ATGTCCACCAAAGGCCCAAA3′	RT-PCR
INSIG2 (mouse)	S 5′GGCGGTGTTCGTGGGTATAA3′ AS 5′TGACGGCCAATGTTTCCCAT3′	RT-PCR	INSIG2 (human)	S 5′GCGGGGGATTTCTGGTAGG3′ AS 5′ACACCGCATTACACTGGACC3′	RT-PCR
LDLR (mouse)	S 5′AGACCCAGAGCCATCGTAGT3′ AS 5′CTCACACCAGTTCACCCCTC3′	RT-PCR	LDLR (human)	S 5′TGTTCCCACGTCTGCAATGA3′ AS 5′GGATGAGGCTGGTGTACTCG3′	RT-PCR
LOX1 (mouse)	S 5′ACTGGCTCTGGCATAAAGAAAAC3′ AS 5′GTAAAGAAACGCCCCTGGTCTTA3′	RT-PCR	LOX1 (human)	S 5′GGCATGCAATTATCCCAGGTG3′ AS 5′TGCCAGATCCAGTCTTGCG3′	RT-PCR
LXRα (mouse)	S 5′AGTGTAACAGGCGCTCCTTC3′ AS 5′TTGGCAAAGTCTTCCCGGTT3′	RT-PCR	LXRα (human)	S 5′ACTGATGTTCCCACGGATGC3′ AS 5′CACAGTGTTAGCGAGGGCT3′	RT-PCR
LXRβ (mouse)	S 5′ACGATCTTTCTCCGACCAGC3′ AS 5′CTGTCTCGTGGTTGTAGCGT3′	RT-PCR	LXRβ (human)	S 5′CACAGTCACAGTCGCAGTCA3′ AS 5′TCGGAGAAGGAGCGTTTGTT-3′	RT-PCR
MMP2 (mouse)	S 5′CCAACTACGATGATGAC3′ AS 5′ACCAGTGTCAGTATCAG3′	RT-PCR	MMP3 (mouse)	S 5′TCCTGATGTTGGTGGCTTCAG3′ AS 5′TGTCTTGGCAAATCCGGTGTA3′	RT-PCR
MMP3 ChIP #1 (mouse)	S 5′AGCCAGTCCTATGATTTTACTTTGAG3′ AS 5′CTTTCCTTTCACCGTGTTAATCC3′	CHiP	MMP3 ChIP #2 (mouse)	S 5′ATTTTAAGTGTGTGCTATATGTCAAG3′ AS 5′CGTTAGACTTCCCTGAGCA3′	CHiP
MMP9 (mouse)	S 5′ACCACATCGAACTTCGA3′ AS 5′CGACCATACAGATACTG3′	RT-PCR	MMP12 (mouse)	S 5′CCCAGAGGTCAAGATGGATG3′ AS 5′GGCTCCATAGAGGGACTGAA3′	RT-PCR
MMP13 (mouse)	S 5′TGATGGACCTTCTGGTCTTCTGG3′ AS 5′CATCCACATGGTTGGGAAGTTCT3′	RT-PCR	MMP13 ChIP #1 (mouse)	S 5′GCCACATCACCTCCAATAAGA3′ AS 5′ACCAGGAACATGTAAATAAGAAAAG3′	CHiP
MMP13 ChIP #2 (mouse)	S 5′TCTATCTGTTTTGCTTTCTCTTAT3′ AS 5′CCATATCTCAAAATCTACCTCC3′	CHiP	RORα (mouse)	S 5′-AAATGAAACAATAACAACGAAGAC3′ AS 5′-TGGACTCTGCTGTTACCCG3′	RT-PCR
RORα (human)	S 5′GCAGATAACGTGGCAGACCT3′ AS 5′GCGATCCGCTGACATCAGTA3′	RT-PCR	RORβ (mouse)	S 5′AGCTGCTTCAACAACGGGCA3′ AS 5′ACCACTTCCAAGCAACCTGA3′	RT-PCR
RORβ (human)	S 5′GGGTTATTACAACGTCGATTCCG3′ AS 5′CGTATTGGATGGCGTGAGTG3′	RT-PCR	RORγ (mouse)	S 5′TGCGACTGGAGGACCTTCTA3′ AS 5′CAGATCCACACCACCGTATT3	RT-PCR
RORγ (human)	S 5′GCTCTGGGCCCTCATATTC3′ AS 5′TGGCATGTCTCCCTGTAGG3′	RT-PCR	SCAP (mouse)	S 5′ACCGCAGCACAGGCATCAAG3′ AS 5′CCAGCACAGAGGGCACATACAC3′	RT-PCR
SCAP (human)	S 5′GCAGCACAGGCATCAAGTTC-3′ AS 5′CCCAAAGTGCCTGACAGATGAT3′	RT-PCR	SCARB1 (mouse)	S 5′CATCGGGCAAACAGGGAAGA3′ AS 5′GAATGGCCTCCTTATCCTGGG3′	RT-PCR
SCARB1 (human)	S 5′AGCAAAACTGTAGGGTCCTGA3′ AS 5′GCACTGAGTCCCCACTGAAT3′	RT-PCR	SOX9 (mouse) (1)	S 5′ATGCTATCTTCAAGGCGCTG3′ AS 5′GACGTCGAAGGTCTCAATGT3′	RT-PCR
SOX9 (mouse) (2)	S 5′CACTGGCAGTTACGGCATCAG3′ AS 5′CATGTAAGTGAAGGTGGAGTAGAGC3′	RT-PCR	SREBP1 (mouse)	S 5′GAGGACATCTTGCTGCTTCTAACC3′ AS 5′GCAATACAGTTCAACGCTCGCTCTAG3′	RT-PCR
SREBP1 (human)	S 5′CACCTGGACCTGGCTTGTAG3′ AS 5′TCCCCATCCACGAAGAAACG3′	RT-PCR	SREBP2 (mouse)	S 5′AAGCTGGGCGATGGATGAGA3′ AS 5′ATGGGACCTGGCTGAATGAC3′	RT-PCR
SREBP2 (human)	S 5′AGCTGACCCTGGGAGACATC3′ AS 5′TGACTTGCAGAGTTGGAGCC3′	RT-PCR	ZIP8 (mouse)	S 5′GAACAATTGCCTGGATGATCACGC3′ AS 5′AAGCCGGTTAACATCCCTGCATTC3′	RT-PCR
CYP7B1 (mouse)	S 5′CCCTATCTTAGTATCTGACAT3′ AS 5′ATGTCAGATACTAAGTATGGG3′	shRNA	LOX1 (mouse)	S 5′CCCUCACCUUGAAGCUGAATT3′ AS 5′UUCAGCUUCCAAGGUGAGGGTG3′	siRNA

S, sense; AS, antisense

nature research

Corresponding author(s): Jang-Soo Chun and Je-Hwang Ryu

Reporting Summary

Nature Research wishes to improve the reproducibility of the work that we publish. This form provides structure for consistency and transparency in reporting. For further information on Nature Research policies, see Authors & Referees and the Editorial Policy Checklist.

Statistical parameters

When statistical analyses are reported, confirm that the following items are present in the relevant location (e.g. figure legend, table legend, main text, or Methods section).

n/a	Confirmed
☐	☒ The exact sample size (*n*) for each experimental group/condition, given as a discrete number and unit of measurement
☐	☒ An indication of whether measurements were taken from distinct samples or whether the same sample was measured repeatedly
☐	☒ The statistical test(s) used AND whether they are one- or two-sided *Only common tests should be described solely by name; describe more complex techniques in the Methods section.*
☐	☒ A description of all covariates tested
☐	☒ A description of any assumptions or corrections, such as tests of normality and adjustment for multiple comparisons
☐	☒ A full description of the statistics including central tendency (e.g. means) or other basic estimates (e.g. regression coefficient) AND variation (e.g. standard deviation) or associated estimates of uncertainty (e.g. confidence intervals)
☐	☒ For null hypothesis testing, the test statistic (e.g. *F*, *t*, *r*) with confidence intervals, effect sizes, degrees of freedom and *P* value noted *Give P values as exact values whenever suitable.*
☒	☐ For Bayesian analysis, information on the choice of priors and Markov chain Monte Carlo settings
☒	☐ For hierarchical and complex designs, identification of the appropriate level for tests and full reporting of outcomes
☒	☐ Estimates of effect sizes (e.g. Cohen's *d*, Pearson's *r*), indicating how they were calculated
☐	☒ Clearly defined error bars *State explicitly what error bars represent (e.g. SD, SE, CI)*

Our web collection on statistics for biologists may be useful.

Software and code

Policy information about availability of computer code

Data collection	1) Image analysis: Image J, version v.1.51a 2) qRT-PCR analysis: StepOne™ Software, version. 2.3 3) Statistical analysis: SPSS statistics, Release. 23.0.0.0 4) Microarray data analysis: R, version.3.3.2; BioConductor, version. 3.4; Affy (R package)-RMA, version. 1.52.0; Python from Python Software Foundation, version. 3.4.3; StatsModels (Python module)-Statistics, version. 0.8.0 5) Protein-Protein interaction visualization Cytoscape-Visualization, version. 3.5.0; STRING-PPI DB, version. 10.0 6) LC-MS/MS analysis: Xcalibur version. 2.2 7) Binding assay of cholesterol and oxysterols: Molecular Devices FlexStation version 3.0 (Molecular Devices)
Data analysis	Image J was used to analyze microscopic images and immunofluorescent images. CFX Connect Real-Time PCR Detection System (Bio-Rad) and StepOne software ver 2.3 was used for data analyses of quantitative PCR. All statistical calculations in the paper were performed using the SPSS statistics, Release. 23.0.0.0. Agilent 1100 series high performance liquid chromatography (HPLC) pump (Agilent Technologies) linear ion trap mass spectrometer (LTQ; Thermo Fisher Scientific) and Xcalibur ver 2.2(Thermo Fisher Scientific) was used for metabolite quantification (LC MS). Cytoscape-Visualization ver 3.5.0 and STRING-PPI DB ver 10.0 were used for protein-protein interaction data analyses. Molecular Devices FlexStaion ver 3.0 (Molecular Device) was used for binding assay of cholesterol and oxysterols to RORalpha. R, version.3.3.2; BioConductor, version. 3.4; Affy (R package)-RMA, version. 1.52.0; Python from Python Software Foundation, version. 3.4.3; StatsModels (Python module)-Statistics, version. 0.8.0 were used for microarray data analysis. GraphPad

Prism 7.00 was used for data analysis of binding assay of cholesterol and oxysterols to RORalpha. OriginPro 2018 (64 bit) SR1 b9.5.1.195 was used as a graphing software.

For manuscripts utilizing custom algorithms or software that are central to the research but not yet described in published literature, software must be made available to editors/reviewers upon request. We strongly encourage code deposition in a community repository (e.g. GitHub). See the Nature Research guidelines for submitting code & software for further information.

Data

Policy information about availability of data

All manuscripts must include a data availability statement. This statement should provide the following information, where applicable:

- Accession codes, unique identifiers, or web links for publicly available datasets
- A list of figures that have associated raw data
- A description of any restrictions on data availability

Microarray data have been deposited in Gene Expression Omnibus with the accession codes GSE104794 (for HIF-2alpha), GSE104795 (for ZIP8), and GSE104793 (for IL-1beta). The following figures have associated raw data: Figures 1a-d, 1f-g, 2b-c, 2f-g, 3a, 3c-e, 4a-b, 4e-f; Extended Data Figures 1a-e, 2d, 4d-e, 4g-i, 5d-g, 6a, 7a-b, 7e-f, 8c, 9b-c, 9e-i, 10a-e, 10g-h. For gel source data, Supplementary Figure 1.

Field-specific reporting

Please select the best fit for your research. If you are not sure, read the appropriate sections before making your selection.

☒ Life sciences ☐ Behavioural & social sciences ☐ Ecological, evolutionary & environmental sciences

For a reference copy of the document with all sections, see nature.com/authors/policies/ReportingSummary-flat.pdf

Life sciences study design

All studies must disclose on these points even when the disclosure is negative.

Sample size	Although no statistical methods were used to predetermined sample size in vitro and in vivo analyses, we conducted preliminary experiments to estimate variances in each assay and determined sufficient sample size.
Data exclusions	No samples or animals were excluded from analyses.
Replication	All experimental findings were reproduced independently at least four times. For each figure panel, the numbers of biologically independent samples, mice per group, or human specimens are indicated in the figure legends. Data shown in figure panels are the mean of all independent biological repeats. Western blot pictures, confocal microscopy images, or histological images typically are from a representative experiment; however, the number of independent repeats is clearly indicated in the figure legends and all attempts at replication were successful.
Randomization	For in vitro experiments, cultures were randomly chosen for different treatments and experiments were performed multiple times. For mouse experiments, mutant mice (Ch25h -/- or RORalpha Sg/+) and WT littermates were allocated into groups based on sex, age, and genotype. Male mice were selected for the experiment in order to avoid concerns about hormonal effect in female mice. After the selection, mice for the DMM surgery, high cholesterol diet, or intra-articular injection were allocated randomly without subjective judgement.
Blinding	Cartilage destruction analysis, synovial inflammation scoring, osteophyte maturity analysis, SBP thickness analysis, and immunohistochemistry were performed by individuals (Wan-Su Choi, Gyuseok Lee, Jiye Yang, Ji-Sun Kwak, Hyo-Eun Kim, Seul Ki Kim) who were blinded to the nature of the mice under analysis (both what specific mouse strains or treatment groups were in the experiment and whether any individual mouse belonged to control versus experimental groups).

Reporting for specific materials, systems and methods

Materials & experimental systems

n/a	Involved in the study
☒	☐ Unique biological materials
☐	☒ Antibodies
☐	☒ Eukaryotic cell lines
☒	☐ Palaeontology
☐	☒ Animals and other organisms
☐	☒ Human research participants

Methods

n/a	Involved in the study
☒	☐ ChIP-seq
☒	☐ Flow cytometry
☒	☐ MRI-based neuroimaging

Antibodies

Antibodies used

Immunohistochemistry
CH25H (1:50; Antibodies online; ABIN1415409; Lot#AE101429)
CYP7B1 (1:50; Thermo Fisher Scientific; PA5-28121; Lot#RI22732539)
HIF-2alpha (1:100; Abcam; ab8365; Lot#GR104042-5)
LOX-1 (1:150; Abcam; ab60178; Lot#GR225261-29)
MMP3 (1: 100; Abcam; ab52915; Lot#GR1299549)
MMP13 (1:100; Abcam; ab39012; Lot#GR149380-1)
RORalpha (1:100; Sigma Aldrich; AV45608; Lot#QC13886)
ZIP8 (1:100; Santa Cruz Biotechnology; sc133415; Lot#D0610)
NITEGE (1:1000; Novus; NB100-74350; Lot#A-2)
DIPEN (1:100; MyBioSource; MBS442010; Lot#S1703003)

Immunofluorescence
LOX-1 (1:400; Abcam; ab60178; Lot#GR225261-29)

Western blotting
COL2A1 (1:1000; Millipore; MAB8887; Lot# 2603842)
ERK1 (1:2000; BD Biosciences; 610408; Lot#3032798)
MMP3 (1:1000; Abcam; ab52915; Lot#GR1299549)
MMP13 (1:1000; Aviva System Biology; ARP56350_P050; Lot#QC27350-100225)
RORalpha (1:1000; Sigma Aldrich; AV45608; Lot#QC13886)
SOX9 (1:1000; Santa Cruz Biotechnology; sc20095; Lot#L1412)

ChIP assay
RORalpha (4 ug/1 ml; Sigma Aldrich; AV45608; Lot#QC13886)

Validation

All antibodies used in this study were validated by the suppliers as follows:
CH25H (1:50; Antibodies onlice; ABIN1415409; Lot#AE101429) for IHC: species (Human, Mouse, Rat), application (WB, IHC-P), manufacturer's website (https://www.antibodies-online.com/antibody/1415409/anti-Cholesterol+25-Hydroxylase+CH25H+AA+58-84+antibody+HRP/)
CYP7B1 (1:50; Thermo Fisher Scientific; PA5-28121; Lot#RI22732539) for IHC: species (Human), application (WB, IHC-P, IF, ICC), manufacturer's website (https://www.thermofisher.com/antibody/product/CYP7B1-Antibody-Polyclonal/PA5-28121)
HIF-2alpha (1:100; Abcam; ab8365; Lot#GR104042-5) for IHC: species (Human, Rat), application (WB, IHC-P, ELISA, Flow Cyt), manufacturer's website (https://www.abcam.com/hif-2-alpha-antibody-ep190b-ab8365.html)
LOX-1 (1:150; Abcam; ab60178; Lot#GR225261-29) for IHC: species (Human, Mouse, Rat, Pig), application (WB, IHC-P, IF, ICC), manufacturer's website (https://www.abcam.com/lox-1-antibody-ab60178.html)
MMP3 (1: 100; Abcam; ab52915; Lot#GR1299549) for IHC: species (Human, Mouse, Rat), application (WB, IHC-P, IF, ICC), manufacturer's website (https://www.abcam.com/mmp3-antibody-ep1186y-ab52915.html)
MMP13 (1:100; Abcam; ab39012; Lot#GR149380-1) for IHC: species (Human, Mouse, Rat, Dog), application (WB, IHC-P, IF, ELISA, ICC, Flow Cyt), manufacturer's website (https://www.abcam.com/mmp13-antibody-ab39012.htm)
RORalpha (1:100; Sigma Aldrich; AV45608; Lot#QC13886) for IHC: species (Human, Mouse, Rat, Dog, Bovine, Goat, Rabbit, Sheep), application (WB, IHC-P), manufacturer's website (https://www.sigmaaldrich.com/catalog/product/sigma/av45608?lang=ko&region=KR)
ZIP8 (1:100; Santa Cruz Biotechnology; sc133415; Lot#D0610) for IHC: species (Human, Mouse, Rat), application (WB, IHC-P, IP), manufacturer's website (https://www.scbt.com/scbt/search?Ntt=sc-133415)
NITEGE (1:1000; Novus; NB100-74350; Lot#A-2) for IHC: species (Human, Mouse, Rat, Bovine, Canine), application (WB, IHC-P, IP, ICC, Flow Cyt), manufacturer's website (https://www.novusbio.com/products/aggrecan-neoepitope-antibody_nb100-74350)
DIPEN (1:100; MyBioSource; MBS442010; Lot#S1703003) for IHC: species (Human, Rat, Guinea pig, Horse, Pig), application (WB, IHC-P, ELISA), manufacturer's website (https://www.mybiosource.com/prods/Antibody/Monoclonal/Aggrecan-N-terminal-neoepitope-DIPEN/ACAN/datasheet.php?products_id=442010)
LOX-1 (1:400; Abcam; ab60178; Lot#GR225261-29) for IF: species (Human, Mouse, Rat, Pig), application (WB, IHC-P, IF, ICC), manufacturer's website (https://www.abcam.com/lox-1-antibody-ab60178.html)
COL2A1 (1:1000; Millipore; MAB8887; Lot# 2603842) for WB: species (Human, Mouse, Chicken), application (WB, IHC-P, IF), manufacturer's website (http://www.merckmillipore.com/KR/ko/product/Anti-Collagen-Type-II-Antibody-clone-6B3,MM_NF-MAB8887)
ERK1 (1:2000; BD Biosciences; 610408; Lot#3032798) for WB: species (Human, Mouse, Rat, Dog, Chicken, Frog), application (WB, IHC-P, IF, IP), manufacturer's website (http://www.bdbiosciences.com/ptProduct.jsp?ccn=610408)
MMP3 (1:1000; Abcam; ab52915; Lot#GR1299549) for WB: species (Human, Mouse, Rat), application (WB, IHC-P, IF, ICC), manufacturer's website (https://www.abcam.com/mmp3-antibody-ep1186y-ab52915.html)
MMP13 (1:1000; Aviva System Biology; ARP56350_P050; Lot#QC27350-100225) for WB: species (Human, Mouse, Rat, Rabbit, Cow, Dog, Guinea pig, Horse, Sheep, Yeast), application (WB), manufacturer's website (https://www.avivasysbio.com/mmp13-antibody-middle-region-arp56350-p050.html)
RORalpha (1:1000; Sigma Aldrich; AV45608; Lot#QC13886) for WB: species (Human, Mouse, Rat, Dog, Bovine, Goat, Rabbit, Sheep), application (WB, IHC-P), manufacturer's website (https://www.sigmaaldrich.com/catalog/product/sigma/av45608?lang=ko&region=KR)
SOX9 (1:1000; Santa Cruz Biotechnology; sc20095; Lot#L1412) for WB: species (Mouse, Rat), application (WB, IHC-P, ICC), manufacturer's website (https://www.scbt.com/scbt/ko/product/sox-9-antibody-h-90)
RORalpha (4 ug/1 ml; Sigma Aldrich; AV45608; Lot#QC13886) for ChIP assay: species (Human, Mouse, Rat, Dog, Bovine, Goat, Rabbit, Sheep), application (WB, IHC-P), manufacturer's website (https://www.sigmaaldrich.com/catalog/product/sigma/av45608?lang=ko&region=KR)

The specificity of CH25H antibodies is verified by the absence of signal in immunohistochemistry in cartilage tissues from Ch25h knock out (Ch25h KO) mice (see Extended Data Fig. 4c). For anti-CYP7B1 antibodies, we verified specificity through immunohistochemistry on cartilage tissues with shRNA silenced expression and/or overexpression (see Extended Data Fig. 5a and c). For anti-RORalpha antibodies, we additionally verified specificity through immunohistochemistry on cartilage tissues from RORalpha mutant (RORalpha Sg/+) or TG mice (see Extended Data Fig. 8b, 9d). In addition, anti-RORalpna antibodies for ChIP assay is validated by immunoprecipitation of the RORalpha overexpression samples with IgG or RORalpha antibody (see Extended Data Fig. 7g).

Eukaryotic cell lines

Policy information about cell lines

Cell line source(s)	HEK293a from Thermo Fisher Scientific (Cat No. R70507) Raw264.7 from ATCC (Cat No. TIB-71)
Authentication	None of these cell lines were authenticated by us.
Mycoplasma contamination	We confirmed that cell lines used were negative for mycoplasma contamination.
Commonly misidentified lines (See ICLAC register)	No commonly misidentified cell lines were used.

Animals and other organisms

Policy information about studies involving animals; ARRIVE guidelines recommended for reporting animal research

Laboratory animals	C57BL/6 male mice (WT, Ch25h-/-, RORαSg/Sg, and RORαSg/+) were subjected to induction of experimental OA. Ch25h-/- mice (Strain# 016263) and RORαSg/+ mice (a spontaneous RORα mutant strain, Strain# 005047) were obtained from the Jackson Laboratory. Homozygous RORαSg/Sg mice exhibit tremors, body imbalance, hypotonia and small size at birth, and die shortly after weaning; in contrast, heterozygous RORαSg/+ mice exhibit normal development. We therefore used RORαSg/+ mice for our experimental OA studies. Cartilage specific RORa Tg mice were generated using the Col2a1 promoter and enhancer. Details are provided in methods section. For primary cell culture, chondrocytes were isolated from the femoral condyles and tibial plateaus of postnatal day 5 WT mice. Experimental OA was induced by DMM (destabilization of the medial meniscus) surgery or IA (intra-articular) knee injection. 10-12 week old male mice were used.
Wild animals	This study did not involve wild animals.
Field-collected samples	This study did not involve animals collected from the field.

Human research participants

Policy information about studies involving human research participants

Population characteristics	International Cartilage Repair Society (ICRS) grade 4 human knee cartilage tissues were obtained from aged 50-74 years old patients. The cartilage tissues offered by these patients were grouped by damaged and undamaged region for the following analysis. All recruited patients did not have rheumatoid arthritis, which disease can affect the cartilage and synovial membrane. The OA patients with metabolic diseases including diabetes and hypertension were not excluded because of the research purposes to elucidate the regulatory mechanism between cholesterol and osteoarthritis. Sex, weight and height of patients were not controlled.
Recruitment	Patients with a osteoarthritis undergoing arthroplasty were recruited for offering the cartilage tissue. Patients diagnosed with International Cartilage Repair Society (ICRS) grade 4 were eligible for cartilage harvesting and following analysis. Institutional Review Board of Wonkwang University Hospital approved the use of these tissues, and written informed consent was obtained from all patients before the operative procedure. Participants were recruited on an "as available" basis by participating surgeons (Churl-Hong Chun). Recruitment bias is unlikely to impact this study as no patient comparisons are performed and no analysis of demographic or clinical covariates on cellular properties is performed.